ADDIS ABABA UNIVERSITY
SCHOOL OF GRADUATE STUDIES
EARTH SCIENCE DEPARTMENT

THERMAL MAPPING AND LINEAMENT ANALYSIS OF ABIYATA AND LANGANO LAKES REGION IN CENTERAL ETHIOPIAN RIFT SYSTEM

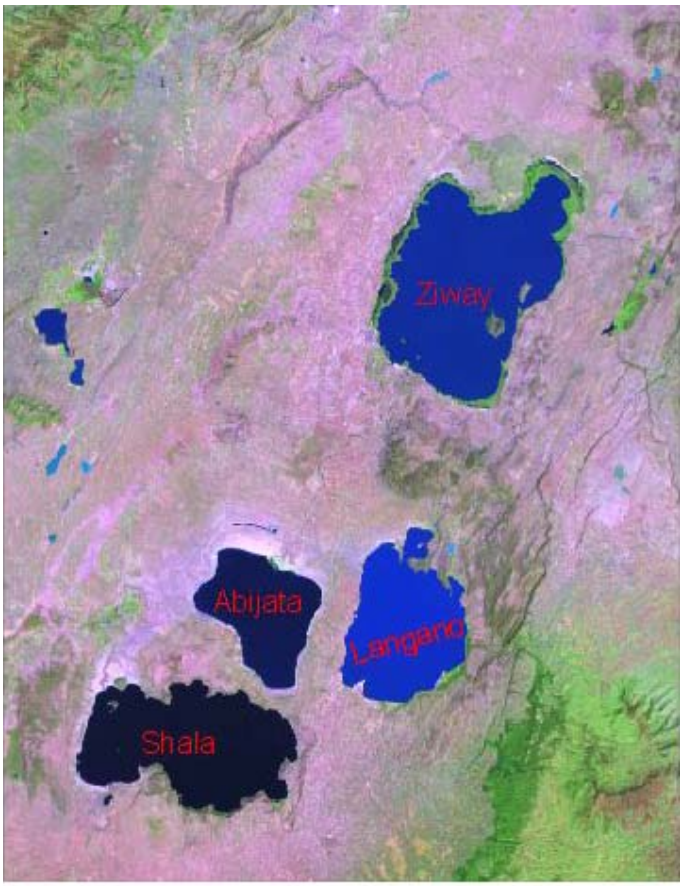

BY

BINYAM TESFAW HAILU

MARCH 2007

THERMAL MAPPING AND LINEAMENT ANALYSIS OF ABIYATA AND LANGANO LAKES REGION IN CENTERAL ETHIOPIAN RIFT SYSTEM

A THESIS SUBMITTED TO THE SCHOOL OF GRADUTE STUDIES ADDIS ABABA UNIVERSITY IN PARTIAL FULFILMENT OF THE REQUIRMENTS FOR THE MASTERS OF SCIENCE DEGREE IN REMOTE SENSING AND GIS

BY

BINYAM TESFAW HAILU

MARCH 2007

ADDIS ABABA UNIVERSITY
SCHOOL OF GRADUATE STUDIES

THERMAL MAPPING AND LINEAMENT ANALYSIS OF ABIYATA AND LANGANO LAKES REGION IN CENTERAL ETHIOPIAN RIFT SYSTEM

By

Binyam Tesfaw Hailu

Department of Earth Sciences

Science Faculty

APPROVED BY BOARD OF EXAMINERS

Dr. Balemwal Atnafu (PhD.) _____

Chairman

Dr. Dagnachew Legesse (PhD) _____

Advisor.

Dr. Bekele Abebe (PhD) _____

Co-Advisor.

Dr. Syed Ali (PhD) _____

Internal Examiner.

Dr. Abera Alemu (PhD) _____

Internal Examiner.

Declaration,

I, the undersigned declare that this thesis is my original work, has not been presented for a degree in any other university and that all sources of material for thesis have been duly acknowledged.

Binyam Tesfaw

School of Graduate Studies
March 2007.

Acknowledgement

I would like to thank Dr. Dagnachew Legesse and Dr. Bekele Abebe in a special way that advised and shared their knowledge, critical reading of the manuscript and their helpful comments give the present form of this thesis. In addition I thank him Mr. Haili Jia , who gave the Visual Basic Scripts for this study , from Department of Earth Sciences, University of the Western Cape, South Africa.

I luckily recognize the Ethiopian Geological Survey, Hydrothermal department and its librarian for their wholehearted and kind collaboration in delivering me the most valuable data even without a brief time of delay, the Awasa T.V.E.T. College for allowing me to pursue my postgraduate studies.

I also would like to forward my heart felt thanks to all the member of MaWari (Management of water resources in the Rift Valley) especially Dr. Tamiru Alemayehu and Dr. Dagnachew Legesse who arranged the field work and gave me materials for fulfilling this thesis. I would like to thank all friends whose name is not mentioned, for their encouragement and material support either through e-mail or in person.

Table of Contents

List of Figures

List of Tables

List of Appendix

Abbrivations

3D	3 Dimensional
DENS_LEN	Density Length
DENS_NUM	Density Number
DN	Digital Number
EARS	East African Rift System
EMR	Electromagnetic Radiation
ENE-WSW	East North East- West South West
ERDAS	Earth Resource Data Analysis System
ETM+	Extended Thematic Mapper plus
E-W	East-West
GIS	Geographic Information System
HCA	Hierarchical Cluster Analysis
IDW	Inverse Distance Weight
IR	Infra Red
LMAX	Radiance Maximum
LMIN	Radiance Minimum
LPGS	Level 1G product Generation System
LST	Land Surface temperature
MAWARI	Management of Water resources of the Rift System
MER	Main Ethiopian Rift
NDVI	Normalized Difference Vegetation Index
NE-SW	NorthEast-SouthWest
NIR	Near InfraRed
N-S	North-South
NUM_PNTS	Number of points
NW-SE	NorthWest-SouthEast
ORIENT	Orientation
SE	South East
SRTM	Shuttle Radar Topographic Mission
SWIR	Short Wave InfraRed

TDS	Total Dissolved Solids
TIR	Thermal Infrared
TM	Thematic Mapper
TOA	Top of Atmosphere
USGS	United States Geological Survey
UTM	Universal Traverse Mercator
UV	Ultra Violet
VBA	Visual Basic for Application
VBE	Visual Basic Editor

Abstract

Land surface temperatures are important in global change studies, in estimating radiation budgets in heat balance studies and as a control for climate models. Land surface temperature with the integration of lineament analysis can also determine ground water occurrence and flow directions in arid and semi arid regions. In this study, determination of land surface temperature and lineament mapping has been carried out using remote sensing and GIS in areas of Lake Abijata and Lake Langano regions in the central part of the main Ethiopian Rift, which lies 180 km south of Addis Ababa. This area is exhibited by high temperature and a step faults or lineaments.

The main objectives of this study are producing maps of thermal manifestations at Langano and Abijata Lake regions, Lineament density mapping with respect to Ground water occurrence and comparative Analysis of Lineaments with that of thermal manifestations. The thermal mapping that has been carried out using the image of LANDSAT ETM+ shows a range of 287 to 311 degree Kelvin: based on this result the highest temperature is on the north top and western side of lake Langano which is the discharge area of the hot thermal springs from the eastern high lands of the main Ethiopian rift system. This area might be the best are for hydrothermal activity point of view. The eastern high land of the central main Ethiopian rift also reveals a high density and a number of intersections in lineaments, which is determined using the application of VBA (Visual basic for Application) macros in ArcGIS software, these lineament density maps with the chemistry of groundwater and orientation maps tell us where the ground water flows and where to construct productive wells in the study area as well as in the main Ethiopian rift system.

CHAPTER ONE

General Introduction

1.1. Back Ground

Remote sensing and GIS techniques are the basic tools for different applications regarding resource management. The satellite images are now recorded very rapidly for mapping land surface temperature as well as extraction of lineaments.

The inter relationship of thermal manifestations and lineaments has its own implications for groundwater studies especially in rift areas. In the rift localizations of groundwater is strongly controlled by the rift faults. They have similar role in the movement and occurrence of ground water.

Land surface temperature and lineament analysis are very important in ground water occurrence studies. Thus, in this study integration of thermal mapping and lineament analysis based on VBA approach for ground water occurrence has been explored, applied and validated on data collected in central rift valley of Ethiopia.

1.2. Objectives

- Producing maps of thermal manifestations at Langano and Abijata Lakes region, Ziway- Shalla Basin, Main Ethiopian Rift based on remote sensing and Geographic Information System.
- Lineament Mapping and Analysis of Langano, Abijata and Shalla lake regions with respect to Ground water manifestation and hot springs using remote sensing and GIS.
- Comparative Analysis of Lineaments with that of thermal manifestation map.

1.3. Specific Objectives

- To show the main importance remote sensing and GIS have on the structural analysis and thermal image analysis with respect to the ground water manifestation.
- Remote sensing data interpretation to prepare thermal map and lineament analysis
- To evaluate the images produced by several enhancement techniques for lineament mapping.
- To show some of the applications of thermal image analysis for ground water occurrence.
- To make analysis of lineament length, lineament density, lineament intersections and lineament orientation from the existing lineaments in the Central part of the main Ethiopian Rift.
- Comparison of lineaments with that of Thermal manifestation.

1.4. Description of study area

The main Ethiopian rift is essentially a graben formed by drifting of the Ethiopian and Somali plates and it commenced during late tertiary times and by the Pliocene (Baker et al., 1972). Since then major uplift and graben faulting have been takes place in NE to SW orientation. Even if several studies have been done in main Ethiopian rift valley, still it is the most important area for scientists.

The Ethiopian Rift System, which represents the northern half of the East African Rift System (EARS), consists of three major rift zones with distinct volcanic and tectonic characteristics that are at different stages of rifting. These are the broadly rifted zone of south-western Ethiopia, the Main Ethiopian Rift (MER) of central Ethiopia, and the Afar Rift Systems. The width of the MER increases from the southern (30-60 km) to the central (65-80 km) and the northern (80-120 km) sectors, and is more than 200-km wide in the southern part of the Afar Rift.

In MER numerous lakes fed by streams from the adjacent rift shoulders and highlands occupy the rift floor in the geologic past (Gasse & Street 1978, Gasse et at. 1980). The present day lakes (e.g., Awasa, Shala, and the Langano-Abijata-Ziway basin) within the central sector filled ancestral depressions of Plio-Pleistocene calderas.

This study also point on the ziway-shala basin in the main Ethiopian rift specifically with in 822240 to 877995 N and 440520 to 496635 E in UTM, which is around 3150-km^2 area (Figure 1). Large-scale normal block faulting has disrupted the volcanic rocks and formed step-faults and horst and graben topography (Figure 2). The basin can be divided into three physiographic

regions: the rift floor, the transitional escarpment and Highlands. Rift escarpment faults have undergone a long period of erosion while those of the rift floor are mostly recent. The rift floor consists mainly of extensive flat lands.

Regionally, the Ziway-shala basins is characterized by a semi-arid to sub-humid climate with mean annual precipitation and mean annual temperature varying from 620mm and 25 ^{o}C close to the lakes (Lake Abijata, Langano, Ziway and Shala) to 1200 mm and 15^{0}C on the humid plateau and escarpments respectively.

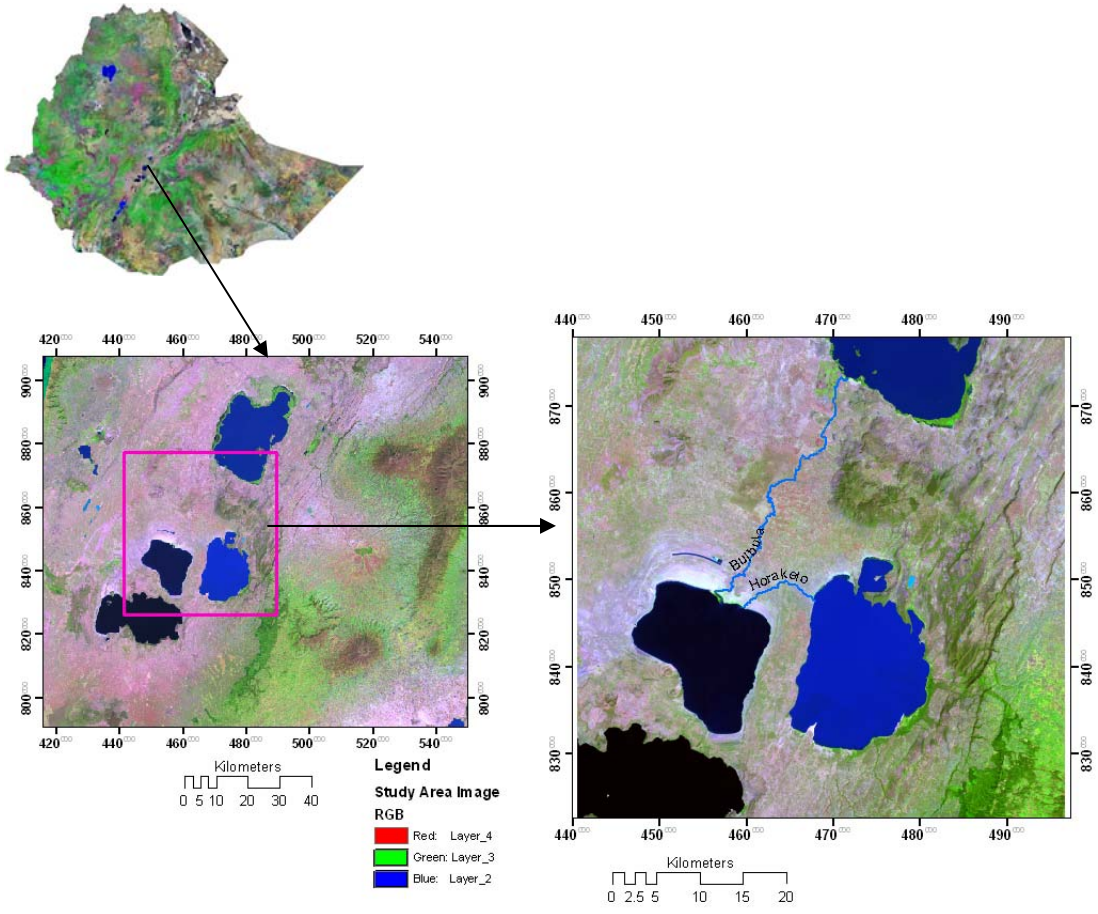

Figure 1: Location map of the study area.

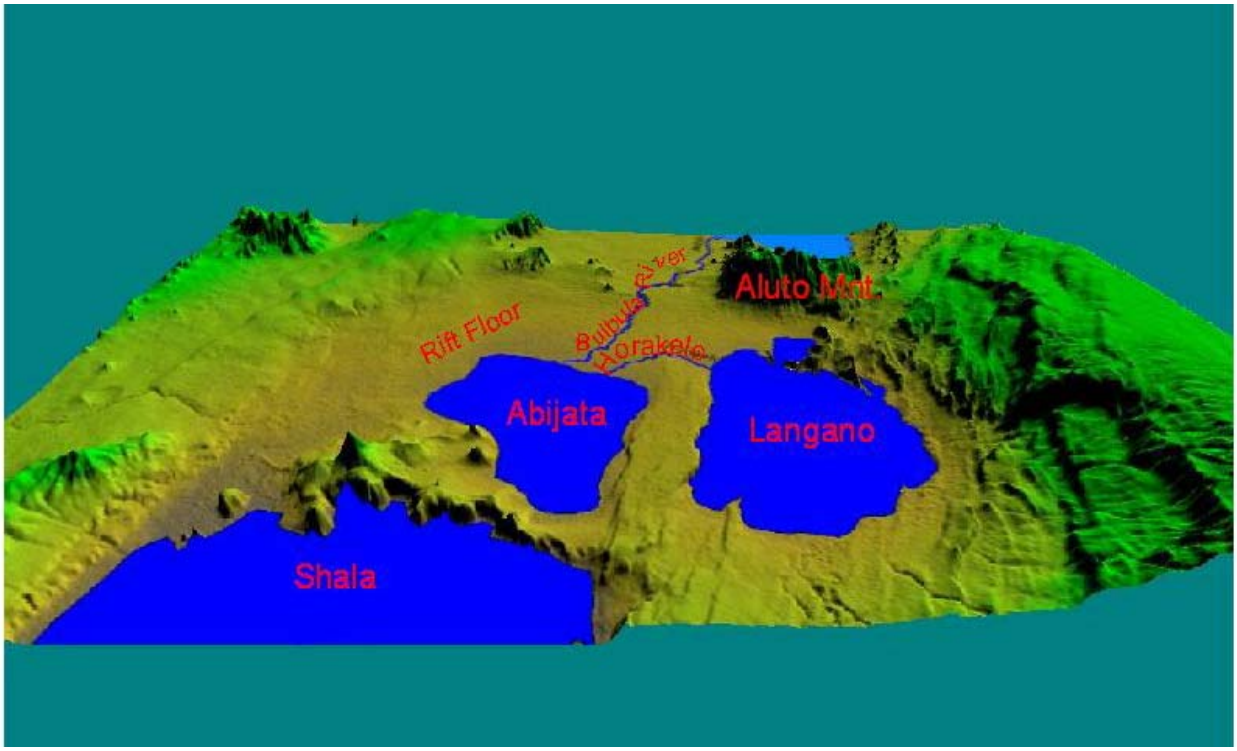

Figure 2: Topographic map of the study area derived from SRTM

As in most of Arid and semi arid lands of African continent (Nicholson and Chervin, 1983), inter annual rainfall variability is inherently extreme in the region. Generally, the pattern of the precipitation in the rift floor is more of stormy type compared to the highlands (Makin et al., 1975)

The vegetation in the rift valley is mainly characterized by Acacia Combertum open woodland, now extensively overgrazed (Woldu and Taddese, 1990) where as deciduous woodlands (Olea europaea, Celtis, Dodonaea uiscosa and Euclea) occupy the escarpments (Mohammed and Bonnefille, 1991)

1.5. Theoretical Background

1.5.1. Remote sensing

Remote sensing is the science of acquiring information (spectral, spatial, and temporal) about the earth's surface without actually being in contact with it. With out direct contact, some means of transferring information through space must be utilised. In remote sensing, information transfer is accomplished by use of Electromagnetic radiation (EMR).

EMR is a form of energy that reveals its presence by the observable effects it produces when strikes the matter. EMR is considered to span the spectrum of wavelengths. Wave length regions of electro-magnetic radiation have different names ranging from gamma ray, x-ray, Ultraviolet (UV), Visible light, infrared (IR), to radio wave, in order from shorter wavelengths (Figure 3)

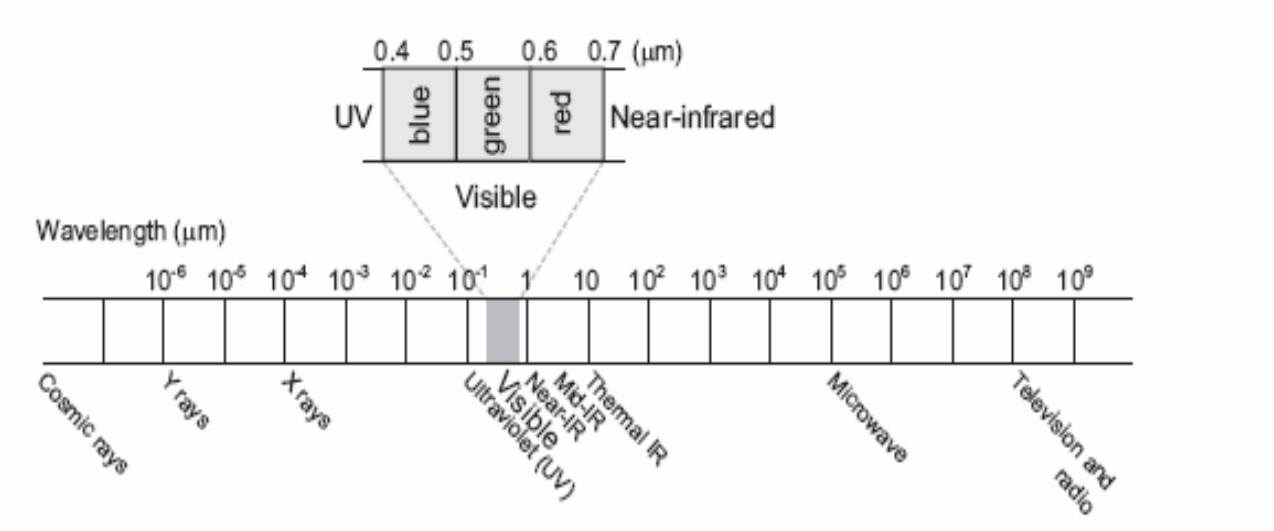

Figure 3: the Electro magnetic spectrum after Thomas M. Lillesand and Ralph W.Kiefer, 1994.

In remote sensing, observation of the earth is carried out using the remote sensing satellites with their remote sensor. Remote sensing satellites are characterized by their altitude, orbit and sensor.

The Landsat program is the oldest earth observation program. It started in 1972 with the Landsat 1satellite carrying the MSS multispectral sensor. After 1982, the thematic Mapper (TM) replaced the MSS sensor. In April 1999 Landsat 7 was launched carrying the ETM+ scanner (table 1). Today, only Landsat-5 and -7 are operational.

System	Landsat-7
Orbit	705 km,98.2o, sun-synchronous,10:00AM crossing,16 days repeat cycle
Sensor	ETM+
Swath width	185 km (FOV =15o)
Off-track viewing	0
Revisit time	16 days
Spectral bands	0.45-0.52(1),0.52-0.60(2),0.63-0.69(3),0.76-0.90(4),1.55-1.75(5),10.4-12.50(6),2.08-2.34(7),0.50-0.90(PAN)
Spatial resolution	15m (PAN),30m (bands 1-5,7),60m(band 6)
Data achieved at	Earthexplorer.usgv.gov

Table 1: Landsat ETM+ characteristics

The application of Landsat thematic Mapper is a lot using each spectral band such as: land cover mapping, land use mapping, soil mapping, geological mapping, surface temperature mapping, mineral mapping, et cetera (Table 2).

Band	Wavelength(μm)	Principal application
1	0.45-0.52	Designed for water body penetration, making it useful for coastal water mapping. Also useful for soil-Vegetation discrimination and forest type mapping
2	0.52-0.60	Designed to measure green reflectance peak of vegetation for vegetation discrimination and Vigour assessment.
3	0.63-0.69	Designed to sense in a chlorophyll absorption region aiding in plant species differentiation.
4	0.76-0.90	Useful for determining vegetation types, Vigour, and bio-mass content, for soil moisture discrimination.
5	1.55-1.75	Indicative of vegetation moisture content and soil moisture. Also useful for differentiation of snow from clouds.
6	10.4-12.50	Useful in vegetation stress analysis, Soil moisture discrimination, and thermal mapping application.
7	2.08-2.34	Useful for discrimination of mineral and rock types. Also sensitive to vegetation moisture content.

Table 2: Principal applications of the Landsat Thematic Mapper bands (from Thomas M. Lillesand and Ralph W.Kiefer, 1994.)

1.5.2. Thermal remote sensing

The wavelength range for infrared region found approximately between 0.70 to 100 mm, which is hundred times wider than the visible portion. Infrared is subdivided mainly in to two parts based on its radiation properties: -

- Reflected infrared
- Emitted or Thermal infrared

Radiation in the reflected infrared region is used for remote sensing purposes in a way similar to radiation in the visible portion and this covers from 0.70 to 3.0 mm where as the thermal infrared region is different from the visible and reflected region, as this energy is essential to the radiation that is emitted from the earth surfaces in the form of heat and this ranges covers between 3.0 to 100mm.

Each energy radiation source or radiator emits a characteristic array of radiation curves. A black body is useful concept, which is widely used by physicists in the study of radiation. Thus from black body radiation can be defined as follows: -

- Sun and earth surfaces behave approximately as black bodies.
- An object, which is perfect emitter, and absorber of radiation.
- For a given temperature and wavelength no surface can emit more energy than a black body.

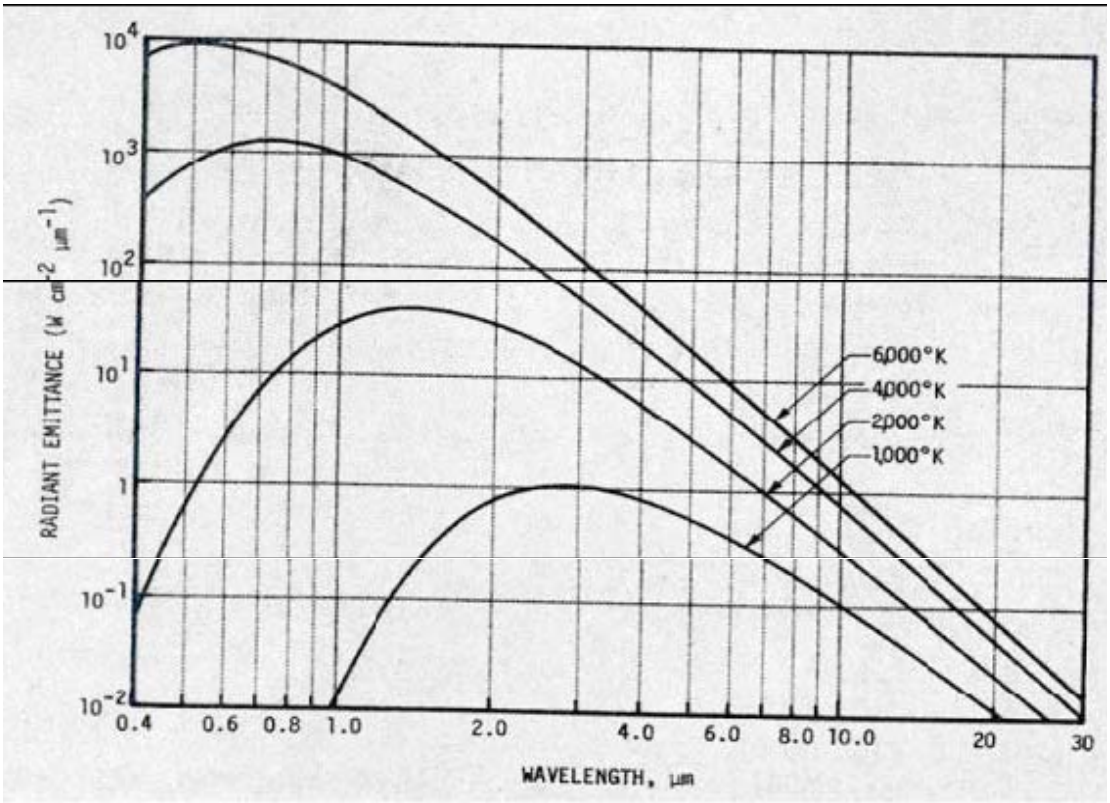

Figure 4: Spectral exitance distributions for blackbodies at 6000, 4000, 2000, and 1000 K.

Thus, a series of laws were derived which relate to compare natural surfaces/radiators to those of black body and explained below.

1.5.2.1. The Planck's Law

Planck's law gives the emissive power of a black body at any wavelength and temperature. For a radiation in to a vacuum or a medium of refractive index of unity, this law in a simple form can be written as follows: -

$$F_{b\lambda} = C_1 / \lambda^5 [e^{C_2/\lambda T_K} - 1] \quad (1)$$

Where

$F_{b\lambda}$ is the hemispherical spectral emissive power of a black body [Wm-2μm-1]

C1 is the first radiation constant [3.7427*108 Wm-2 μm4]

C2 is the second radiation constant [1.4388*104 μmK]

λ is the wavelength [μm]

T_k is the black body temperature [K]

In general, three basic points can be extracted from equation above: -

- The emissive power increases with temperature at each wavelength.
- Relatively more energy is emitted at shorter wavelengths (area under curves).
- The position of the maximum emissive power (maximum peaks) shifts towards shorter wavelengths

1.5.2.2. Wien's Law

Most objects emit radiation at many wavelengths. However there is one wavelength that a given object can emits the highest amount of radiation. The Planck's law can be put in a more universal form dividing by T_k

$$F_{b\lambda} / T_k^5 = C_1 / (\lambda * T_k)^5 * [e^{C_2/\lambda T_K} - 1] \quad (2)$$

The above equation can be expressed $F_{b\lambda} / T_k^5$ in terms of a single variable $\lambda * T_k$ Plotting this equation as a function of $\lambda * T_k$, then the result shows that a maximum peak occurs at: - $\lambda_{\max} * T_k$ =2897.8 μmK.

$$\lambda_{\max} = 2897.8 \mu mK / T_k \quad (3)$$

From Figure 4 above and based on Weins displacement formula above, the earth and the sun can emit the highest radiation at 9.7 μm and 0.48 μm wavelengths respectively.

1.5.2.3. Stefan Boltzman Law

The total surface under the spectral radiant exitance curve shown in Figure 4 above will represent the total amount of radiant energy coming from the black body for the spectral band of all wavelengths. The total surface under the spectral radiant exitance curve shown in Figure 4 above will represent the total amount of radiant energy coming from the black body for the spectral band of all wavelengths.

$$F_b = \int_{\lambda=0}^{\lambda=\infty} F_{b\lambda} * d\lambda = \int_{\lambda=0}^{\lambda=\infty} C_1 / \lambda^5 [e^{(C_2/\lambda * T_k)} - 1]$$

$$= C_1 * \pi^4 * T_k^4 / 15 * C_2^4$$

$$= \sigma * T_k^4 \quad (4)$$

Where

F_b is the total amount of energy at temperature, T [Wm^{-2}]

λ is wavelength [m]

σ is Stefan boltzman constant [$5.67*10^{-8}$ $Wm^{-2}K^{-4}$]

1.5.2.4. Energy emitted by grey and real bodies.

Real bodies resemble more to grey bodies. They allow some energy to be reflected back or pass through them. Not all-incoming energy is used to raise their internal temperature. The kinetic temperature of a real body is always less than the one of the black body of similar characteristics that receives the same energy. Emissivity is the ratio of emittance of a given object and a theoretical black body at the same temperature. The emissivity of a theoretical black body is defined as one and a perfect reflector as zero. The emissivity is always less than one and greater than zero. Since, a black body absorbs all the energy that reaches it; it radiates a maximum heat flux compatible with its internal temperature. A black body then is considered to have a radiant temperature equal to its internal body temperature. The emissivity of a black body is one.

A real body at the same internal temperature radiates less than a black body. When aiming to the real bodies with thermal radiometer they show a radiant temperature lower than its internal or kinetic temperature.

$$T_r = (\varepsilon)^{0.25} * T_k \qquad (5)$$

Thermal radiometer will allow us to determine the surface temperature of a terrestrial object if the emissivity of the object is known.

One of the first uses of thermal images in ground water hydrology is to detect temperature contrasts due to up-welling ground water bodies using thematic mapper data (Meijerink;1996). In some later studies, such contrasts are associated with groundwater discharge areas (Bobba et al., 1992; Batelaan et al., 1993; Tenalem Ayenew, 1998). Short-wave thermal infra-red data have also been used to discover high temperature thermal events and for geothermal resources assessment (Rothery et al., 1988)

1.6. Literature Review

The Ziway-Shala basin occupies shallow tectonic depressions on the floor. Ephemeral lakes have occupied the basin since earlier stages of its development and contributed sediment to the rift floor. Volcanic rocks, erupted centers with in and outside the rift are interbeded with the sediment. These quaternary sediment and volcanic sequence is believed to overlie Mesozoic Sand stone, tertiary trap basalt and tertiary ignimbrite that has been down faulted in to the rift. The ignimbrite forms the high escarpments that bound the rift east of Aluto Volcanic Center. Volcanic and tectonic processes are responsible for creating scenic topographic features and fertile regions, as is the case with the MER. Apart from the presence of rich volcanic soil with great agricultural potential; the basin contains abundant resources of industrial minerals, geothermal energy, and surface and ground water. (Lloyd, 1977)

With in the study area faults are well developed and are responsible for the slightly sinuous western shore of Lake Langano. To the south-southwest the swarm passes just east of Shala caldera, apparently unaffected by tectonics controlling the cauldron subsidence. The normal faults degenerate south of Lake Shala in to deep tensional fissures and collapse lineaments, and the sector dies out SE of Lake Shala. (Lloyd, 1977)

Groundwater in the basin of Ziway-shala moves towards Lake Shala which has the lowest elevation in the area, 1550 meters above sea level How ever, it has been inferred that some groundwater flow from Lake Awasa basin towards lake Shala (Tenalem Ayenew, 1998). Much of the water-bearing zones in the high lands are within the weathered volcanic sequence and locality in interbeded river gravels and alluvial deposits.

In addition, the hydrothermal activities in the study area are those hot springs and fumaroles. These occur at four localities. (Lloyd, 1977)

1. Tulu Godo Island in lake Ziway
2. Aluto Volcano Centre, North Shore of Lake Langano.
3. Shala caldera
4. Corbetti caldera and Corbetti-shala sector of Wonji Fault Belt

However, this study focused on the Aluto Volcanic Centre and northern Shore of Lake Langano while mapping of thermal manifestation in the Ziway-shala basin.

The Aluto volcanic complex is a quaternary volcanic centre located along the Wonji Fault Belt in the central sector of the MER. The oldest out cropping rocks in the area are found at the adjacent eastern rift escarpment and consist mainly of silicic volcanics commonly known as the tertiary ignimbrite unit. This unit is overlain by a fissural basaltic unit known as Bofa basalt, which in turn is covered by sediments of lacustrine origin that extend over large areas of the rift floor. The volcanic products of Aluto volcanic centre itself consist of a succession of ash-flow tuffs, silicic tuff breccias, silicic domes and unwelded pumice flows. These volcanic products are very young and are associated with surface thermal manifestations that consist of hot springs and fumaroles with temperature up to 95^0C, steaming grounds, silica sinter and travertine deposits. The hydrothermal deposit temperatures measured in the deep exploratory wells ranging from 88 to 335^0C (Gianneli and Meseret Teklemaiam, 1993).

Linear features on the surface of the earth have attracted attentions of geologists for many years. This interest has grown most rapidly since the introduction of aerial photographs and satellite image in to geological studies. In the early and middle of 1990s, several geologists, Hobbs (1904, 1992), O'Leary et al. (1976), recognized the existence and significance of linear geomorphic features that were the surface expression of zones of weakness or structural displacement in the crust of the earth. More over, Satellite lineaments are linear features on the earth's surface, usually related to the sub-

surface phenomena. In areas of gently folded or horizontal strata, lineaments are related to fractures and faults, and their orientation and number give an idea of the fracture pattern of rocks (Arlegui and soriano, 1998; Cortes et al., 1998).

Lineaments have been used in many applications: petroleum and mineral exploration, nuclear energy facility sitting, and water resources investigations. Previous studies have revealed a close relationship between lineaments and ground water flow and yield (Lattman and Parizek, 1964; Mabee et al., 1994; Magowe and Carr, 1999; Fernandes and Rudolph, 2001). Some researchers studied relationships between ground water productivity and the number of lineament with in specifically designated areas or lineament density rather than the lineament itself (Hardcastle, 1995).

In the rift localizations of groundwater is strongly controlled by the rift faults. They have contrasting role in the movement and occurrence of ground water. The majority of faults are conduits to ground water flow. In places these open faults allow significant amount of preferential ground water flow parallel and sub-parallel to the rift axis. In the rift valley the direction of groundwater is strongly governed by the orientation of faults, which is often perpendicular to the regional groundwater contours in the highlands and escarpments.

In contrast to the high hydraulic conductivity of the rift fractured volcanics, some faults act as barriers of groundwater flow. This is common case in areas of rift-in-rift structures where the faults deep against the topographic slope forming local graben and horsts.

Therefore mapping of lineament closely related to ground water occurrence and yield is essential to ground water surveys, development, and management. The lineament maps as a thematic map include lineament map, lineament length, lineament density map, lineament intersection map, and other lineament

related maps. The purpose of this study is Lineament Mapping and Analysis of Langano, Abijata and Shalla lakes region with respect to Ground water manifestation and hot springs using remote sensing and GIS.

The use of thermal infra red data is becoming increasingly useful for measuring different surface flux densities and temperatures (Menenti, 1984; Bastiaanssen, 1995; Pelgrum and Bastiaanssen, 1996).One of the application is to study the geothermal manifestations in relation to the rift geologic structure: The study area is characterized by many hot springs and fumaroles associated with geothermal fields. This helps to detect possible migration routes of groundwater. Spring discharges emanating below the lakes could also be estimated from thermal images.

1.7. Materials and Methodology

For this study the materials used are satellite images of Landsat 7 for the thermal mapping and lineament extraction in the study area.

LANDSAT Enhanced Thematic Mapper Plus (ETM+) image (path/row of 168/054 and 168/055) dated on December 03, 1999 was used for the thermal mapping of the study area. (Table 3)

ID	Type	Level of product	Time	Infrared bands	Date	Resolution
1	LANDSAT7 ETM+ (path/row:168/054)	L1G	10:00AM	band 6 Low/high gain	Dec 03, 1999	60m
2	LANDSAT7 ETM+ (path/row:168/055)	L1G	10:00AM	band 6 Low/high gain	Dec 03, 1999	60m

Table 3: description of the image used for the thermal mapping

LANDSAT 7 was launched in April 15, 1999 and captures images of large areas of the sunlit Earth daily by revisiting the same areas at every 16 days. It has an ETM+ sensor, a multi spectral scanning radiometer with eight bands and being capable of providing high resolution image information of the earth's surface. The special resolution of the ETM + sensor is 15m in the panchromatic band; 30 meters in the 6 visible, near and short wave infrared bands; and 60 meters in the thermal infra red band (Table 4). The increased spatial resolution of the thermal infrared band makes it possible to do the more detailed analysis of the thermal imagery than that of TM.

Wavelength regions	Band Number	Spectral Range(μm)	Spectral Resolution (meter)	Swath Width (km)
Visible	1	0.45-0.52	30	183*170
	2	0.53-0.61		
	3	0.63-0.69		
NIR	4	0.78-0.90		
SWIR	5	1.55-1.75		
	6	2.09-2.35		
TIR	7	10.4-12.5	60	
Panchromatic	8	0.52-0.90	15	

Table 4: Spectral Considerations of LANDSAT 7 ETM+.

The data acquisition date has a highly clear atmospheric condition and the image is acquired through the USGS earth Resources Observation System Data Center, which is also radiometrically and geometrically corrected LANDSAT-7 data (level-1G products). And the LANDSAT image was further rectified to a common Universal Traverse Marketer Coordinate System.

There are many applications of Landsat thematic Mapper data, land cover mapping, land use mapping, soil mapping, geological mapping, surface temperature mapping, *et cetera*. Landsat thematic Mapper is the only non-meteorological satellite that has a thermal infrared band

For LANDSAT Thermal imagery, which has a wave length, rang of 10.44-12.42 μm, there is a quantitative analysis before using for thermal mapping (Figure 5).

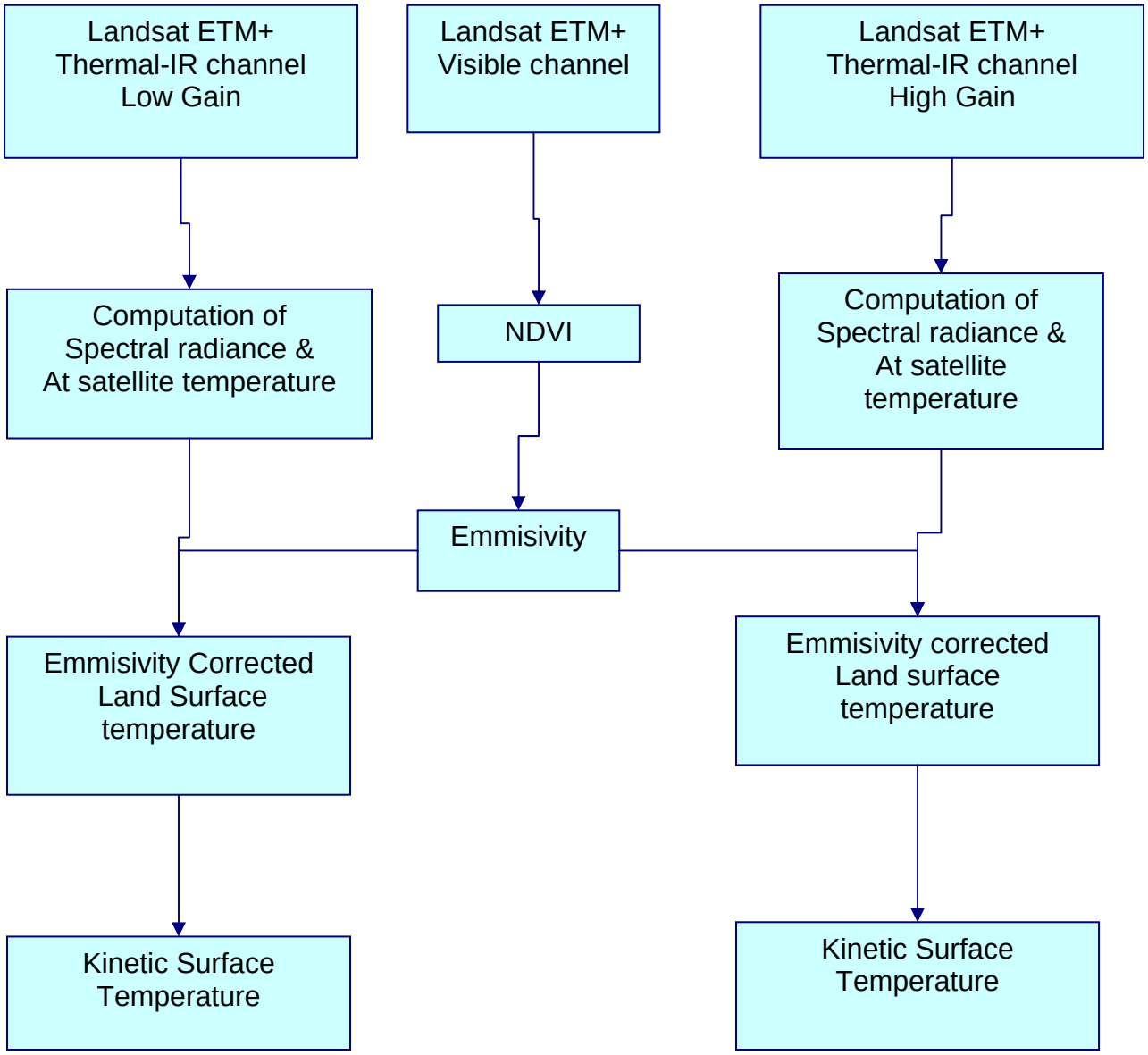

Figure 5: General approach and Methodology used for estimating surface kinetic temperature and emmisivity using LANDSAT 7.

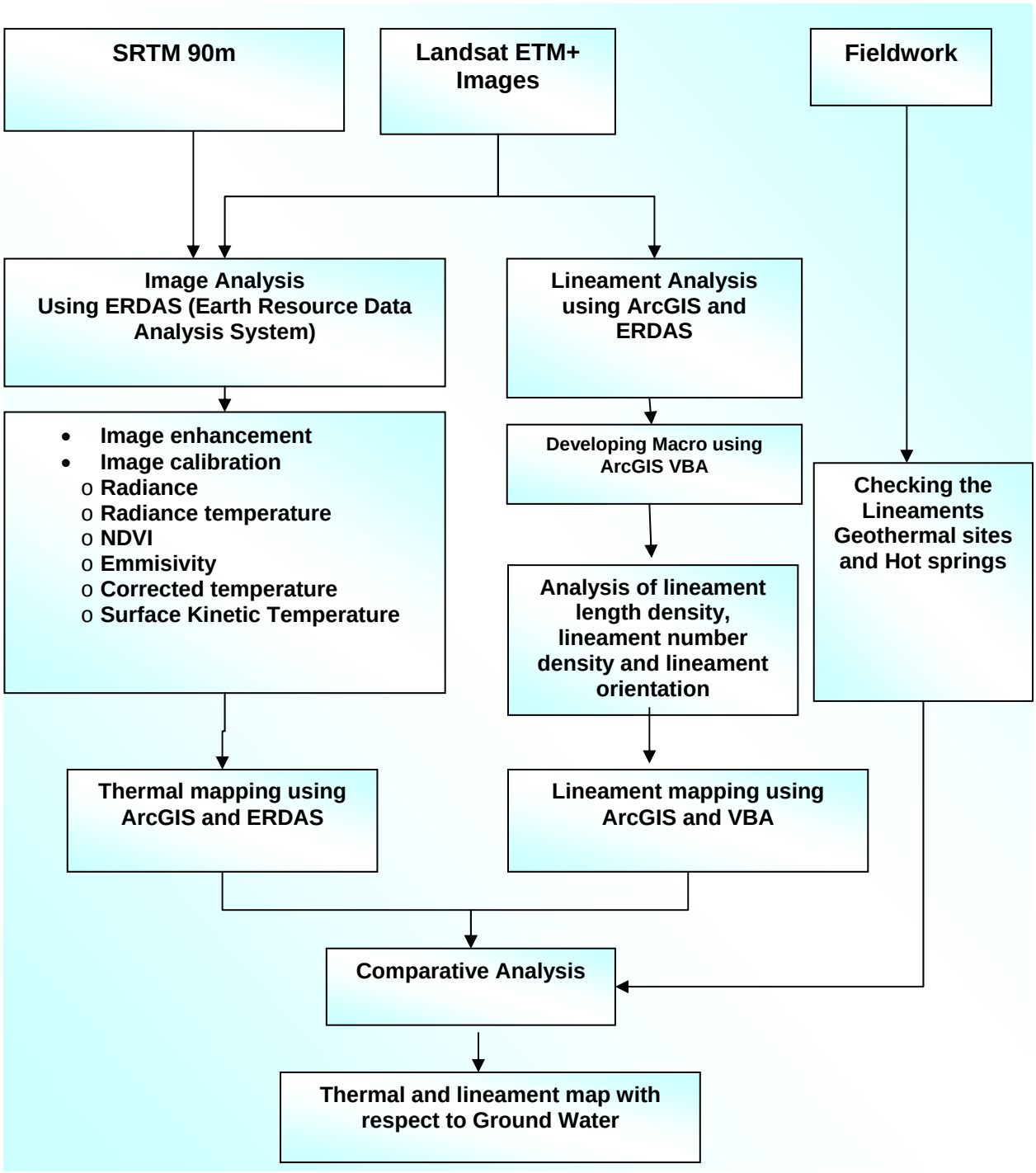

Figure 6: General methodology and materials used structure for this thesis work.

CHAPTER TWO

Data Analysis

2.1. Image processing for thermal mapping

Satellite TIR sensors measure top of the atmosphere (TOA) radiances, from which brightness temperatures (also known as blackbody temperatures) can be derived using Plank's law (Dash et al., 2002). The TOA radiances are the mixing result of three fractions of energy: (1) emitted radiance from the Earth's surface, (2) up welling radiance from the atmosphere, and (3) down welling radiance from the sky. The difference between the TOA and land surface brightness temperatures ranges generally from 1 to 5^{o} K in the 10–12 µm spectral regions, subject to the influence of the atmospheric conditions (Prata et al., 1995). Therefore, atmospheric effects, including absorption, upward emission, and downward irradiance reflected from the surface (Franca & Cracknell, 1994), must be corrected before land surface brightness temperatures are obtained. These brightness temperatures should be further corrected with spectral emissivity values prior to the computation of LST to account for the roughness properties of the land surface, the amount and nature of vegetation cover, and the thermal properties and moisture content of the soil (Friedl, 2002).

Two approaches have been developed to recover LST from multispectral TIR imagery (Schmugge et al., 1998). The first approach utilizes a radiative transfer equation to correct the at-sensor radiance to surface radiance, followed by an emissivity model to separate the surface radiance into temperature and emissivity (Schmugge et al., 1998). The second approach applies the split-window technique for sea surfaces to land surfaces, assuming that the emissivity in the channels used for the split window is similar (Dash et al., 2002). Land surface brightness temperatures are then calculated as a linear combination of the two channels. A major disadvantage of this approach is that

the coefficients are only valid for the data sets used to derive them (Dash et al., 2002).

In other words, a set of thermal responses for a specific landscape phenomenon or process measured using a specific TIR sensor cannot be extrapolated to predict the same TIR measurements either from other sensors, or from images recorded at different times using the same sensor (Quattrochi & Goel, 1995).

In this study the approach has been used by converting the thermal band of Landsat 7 to radiance followed by calculating the at satellite temperature. Then, the satellite temperature is corrected using the emmisivity values, which is computed from the Normalized deference vegetative index, to find the corrected at satellite temperature. And finally that corrected at satellite temperature is changed in to kinetic surface temperature.

2.1.1. Conversion of DN Values to Radiance

The first step is that conversion of DN values to Absolute radiance. The ETM+ images are acquired in either a low or high gain state. The science goal in switching gain states is to maximize the instrument's 8-bit radiometric resolution with out saturating the detectors. This requires matching the gain state for a given scene to the expected brightness conditions. For all LANDSAT ETM+ bands, the low gain dynamic range is approximately 1.5 times the high gain dynamic range. When the surface brightness is high, the sensor image in low gain mode .It is in high gain mode when the surface brightness is lower.

The Digital Number value of the image is converted to the radiance units using equation (6) for low gain and high gain mode of band 6 image.

$$L_\lambda = \left[\left(\frac{L_{\max} - L_{\min}}{Q_{CALMAX} - Q_{CALMIN}} \right) * \left(Q_{CAL} - Q_{CALMIN} \right) + L_{MIN} \right] \qquad (6)$$

Where: L_λ ➔ Radiance

L_{max} ➔ is the radiance at the maximum quantized

L_{min} ➔ is the radiance at the minimum quantized

Q_{CALMAX} ➔ Maximum Quantized and calibrated data digital number= 255

Q_{CALMIN} ➔ Minimum quantized and Calibrated data digital Number= 1 for LPGS (Level 1G product Generation System)

Q_{CAL} ➔ Digital Number

The following table lists two sets of LMIN and LMAX s for band 6 high gain and low gain images.

Spectral Radiance Range (watts/(m^2 *ster*µm))								
Band Number	**Before July 1, 2000**				**After July 1, 2000**			
	Low Gain		**High Gain**		**Low Gain**		**High Gain**	
	LMIN	**LMAX**	**LMIN**	**LMAX**	**LMIN**	**LMAX**	**LMIN**	**LMAX**
6	0.0	17.04	3.2	12.65	0.0	17.04	3.2	12.65

Table 5: LANDSAT7 ETM+ Spectral Radiance Range (USGS)

Since the image is acquired before July 1, 2000 the above values from the table are used for computing the radiance. Further more for the band 6, a bias was found in the pre-launch calibration by a team of independent investigators post launch. For data processed before this, the image radiances given the above transform are 0.31 watts/ (m2 *ster*µm) too high. So that there is a subtraction of 0.31 watts/ (m2 *ster*µm) after conversion.

2.1.2. Conversion of radiance to at Satellite temperature

The second step during quantitative analysis is that conversion of radiance to temperature. The at-satellite temperature can be calculated under an assumption of unity emmisivity and using the pre-launch calibration constants K1 and K2 (LANDSAT Project Science office, 2002). The conversion formula is

$$T = \frac{K2}{\ln\left(\frac{K1}{L_\lambda} + 1\right)} \qquad (7)$$

Where T ➔ Effective at-satellite temperature in Kelvin

K1 ➔ Calibration constant 1 from table below

K2 ➔ Calibration Constant 1 from table below

L_λ ➔ Spectral Radiance

ETM+ Thermal band calibration Constants		
Constants	Values	Units
K1	666.09	watts/(m2 *ster*µm)
K2	1282.71	Kelvin

Table 6: ETM+ Thermal Band Calibration Constants (USGS)

2.1.3. Estimation of emmisivity

However the above temperature values obtained are referenced to a black body, correction for spectral emmisivity become necessary according to the nature of land cover.

Emmisivity is one of the thermal properties of terrain materials which is the efficiency that an object radiates energy. And for perfect absorber or black body the emmisivity is 1, for perfect reflectors or white bodies emmisivity is 0 but for gray bodies emmisivity is between 0 and 1.

The factors influencing emmisivity are tone of objects: darker objects are better absorbers and better emitter, surface roughness: the rougher the surface relative to the wavelength the greater the surface area and greater the potential for absorption and re-emission, moisture content: the more moisture content, the greater the ability to be a good emitter and Field of view and viewing angle can affect the emmisivity.

The effect of land surface emmisivity on satellite measurements can be generalized into three categories: (1) emmisivity causes a reduction of surface-emitted radiance ;(2) non-black surfaces reflect radiance; and (3) the anisotropy of reflectivity and emmisivity may reduce or increase the total radiance from the surface (Patra, 1993). Therefore, retrieval of LST from multispectral TIR data requires an accurate measurement of emmisivity values of the surface (Caselles et al., 1995). The emmisivity of a surface is controlled by such factors as water content, chemical composition, structure, and roughness (Synder et al., 1998). Estimation of emmisivies for ground object has been measured using different techniques such as: NDVI method (Valor and Caselles, 1996)

An emmisivity ε_o for the 8-14 µm spectral range, in which thermal band 10.44-12.42 µm is included, could be predicted from NDVI (Normalized Difference Vegetation Index) Van de crried & Owe, 1992 using

$$\varepsilon_{o(x,y)} = 1.009 + 0.047 \ln NDVI_{(x,y)} \quad (8)$$

Where: $\varepsilon_{o(x,y)}$ = emmisivity of each pixel values

$NDVI = (Band4 - Band3)/(Band4 + Band3)$

The application of the above equation is used for the measurements conducted in NDVI = 0.16 – 0.74.

2.1.4. Land Surface temperature

Land surface temperature then is computed from calculated emmisivity values and calculated temperature at satellite using equation 9 which gives an emissivity corrected image.

$$T_{LST} = \frac{T_B}{1 + (\lambda T_B / \rho) * \ln \varepsilon} \quad (9)$$

Where

λ → Wavelength of emitted radiance

$\rho = hc/K$ (1.438×10^{-2} mK)

h→ Plank's constant (6.26×10^{-34} J-sec).

c→ Velocity of light (2.998×10^{8} m/sec)

K→ Stefan Boltzmann's Constant (1.38×10^{-23} J/K)

2.1.5. Surface Kinetic Temperature

The electromagnetic radiation exiting an object is termed radiant flux. The radiant temperature is highly correlated to the kinetic temperature. Thermal infrared system records radiant temperature. For a black body, the radiant temperature is the same as the kinetic temperature. But for gray body, their

relationship is expressed as shown in equation (5) and it is possible to find the Kinetic temperature of the object.

2.2. Lineament Analysis

2.2.1. Preparation of Lineament map

Lineaments have been screen digitized from the existing 1:500,000 scale structural map of the main Ethiopian rift (Bekele et., al.,2000) and additional lineaments extracted from the LANDSAT ETM+ image using spatial filtering and edge enhancement technique in ERDAS software.

Spatial filtering and edge enhancement are mathematical convolution methods that act on neighboring pixels of digital image. The highlight linear features such as: faults, dykes, regional lineaments and major lithologic boundaries. Directional filters with high-pass spatial filter applied on digital images to increase the visibility of linear features such as faults in specific directions.

The standard techniques include an initial stage of image processing using high-pass and directional filters that detect edge in the preferred orientation. It consists of selectively enhancing the high-, Medium- and low-frequency variations of digital number (DN) in an image.

Emphasizing the spatial frequency component of an image can further enhances obscure features or peak out features of interest hidden within a cluttered, highly textured, original image. This may be done by masking out part of the Fourier transform of the image, or more simply by passing rectangular kernels filter over the image. A mathematical technique for separating an image into its various spatial frequency component is Fourier analysis (Lillesand and Kiefer, 1994). According to Lillesand and Kiefer (1994), a high-pass and directional filter is a type of Fourier transform that enable high frequencies, amplitude and direction of an image to be emphasize by algorithm

known as filters. A common filtering procedure involves moving a window of a few pixels an in dimension (e.g. 3X3, 5X5, etc.) over each pixel in the image, applying a mathematical calculation using the pixel values under that windows, and replacing the central pixel with the new value. The window is over along both the row and column dimensions one pixel at a time and the calculations is repeated until the entire image has been filtered and new enhanced image has been generated.

The following high pass directional filtering kernels to enhance the structures in the specific study area have used.

1	0	1
2	0	2
1	0	1

A) North-South Kernel

-1	-2	-1
0	0	0
1	2	1

B) East-West Kernel

2	-1	0
-1	0	1
0	1	2

C) NorthEast-SouthWest Kernel

0	-1	-2
1	0	-1
2	1	0

D) NorthWest-SouthEast Kernel

Table 7: High pass directional filtering kernels used for extracting of additional lineaments in the study area with a scale of 1:100000

Using the extracted lineaments and digitized lineaments , there has been developed macros (Appendix 1, Appendix 2 and Appendix 3) using ArcGIS 9.1 VBA (Visual Basic Application) for performing the objective concerning the lineament analysis with respect to Ground water potential on the study area. Using the program, lineament length density, lineament number density and lineament orientation mapping has been carried out.

The extracted lineaments for the specific area of interest in combination with the digitized lineaments as shown in the Figure 7 have been used as a lineament feature that appears as a second layer in ArcMAP of ArcGIS 9.1 software for the lineament analysis and the study area image is converted to grids of equal size with a 5km width (Figure 8) which appears as a first layer in the ArcMAP.

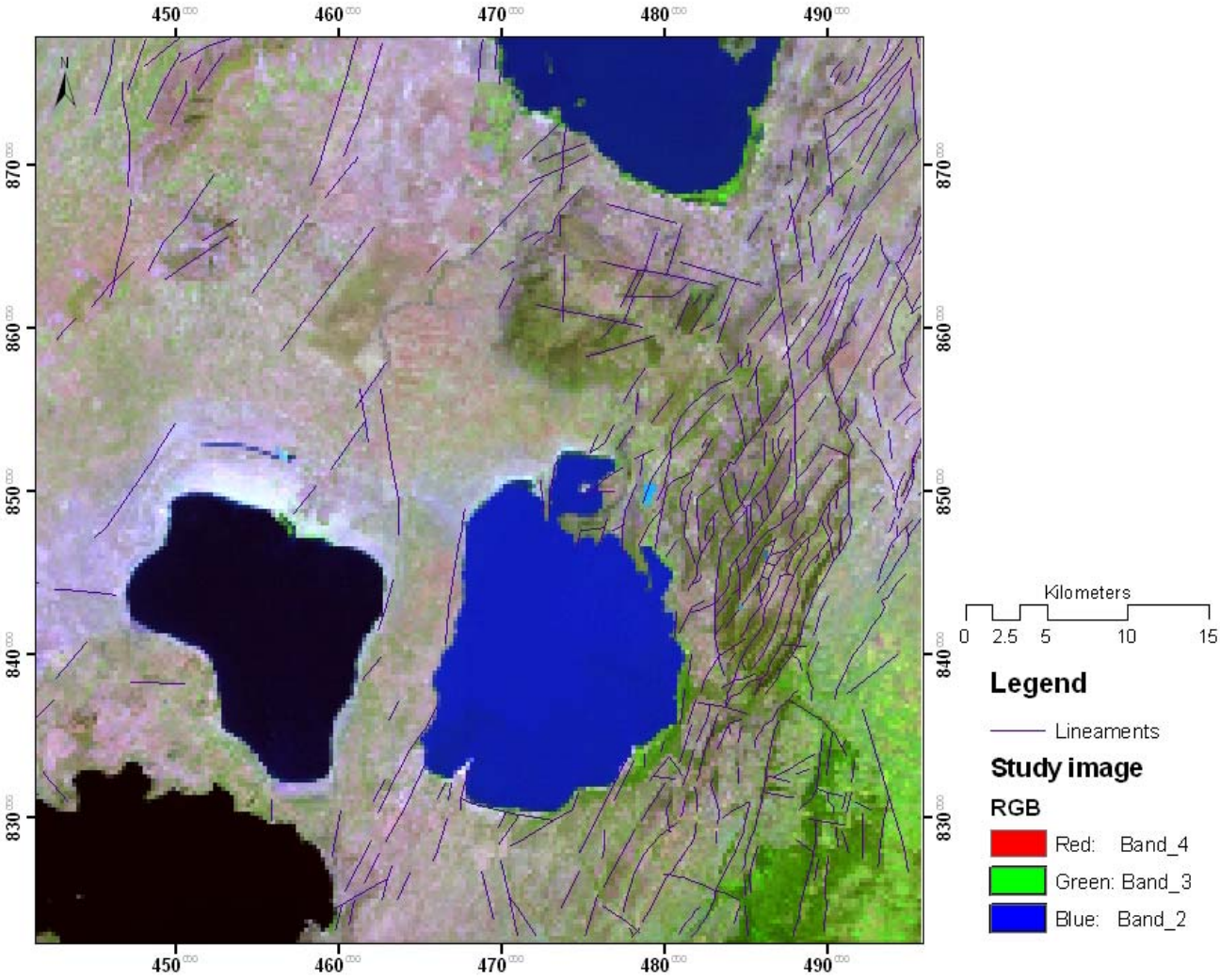

Figure 7: Lineament map of the Langano and Abijata lakes region digitized from the structural map of the central Ethiopian rift

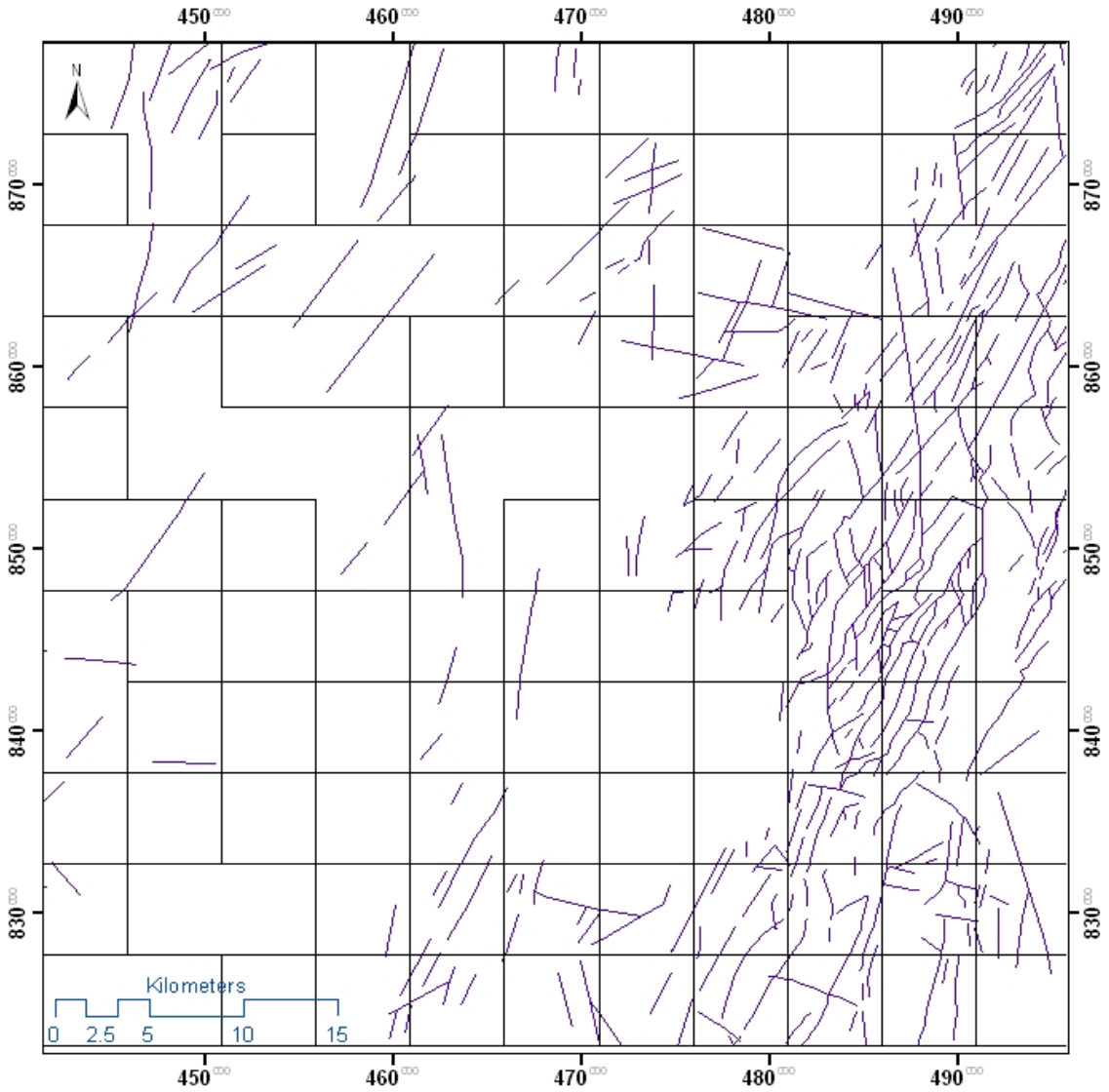

Figure 8: The grid that is computed with 5km width for calculating the lineament density

There have been added fields with a field name of DENS_LEN and DENS_NUM in the polygon attribute table for putting the output data that have been processed using the ArcGIS VBA. In addition, ORIENT and NUM_PNTS have been added to the lineament attribute table.

2.2.2. Development of VBA scripts for lineament Analysis

Both ArcMap and ArcCatalog of the ArcGIS are with Visual Basic for Applications (VBA).VBA is not a standalone program; it's embedded in the application softwares. It provides an integrated programming environment, the Visual Basic Editor (VBE), which lets to write a Visual Basic (VB) macro.

VBA offers a quick and easy entry point for ArcGIS development. The simplest customization through code is the creation of VBA macros, also called procedures that can be run with in the VBA development or by calling the macro from the desktop application. The macro contains VBA code, which uses Arc Objects to perform operations and can also include calls to existing ArcGIS desktop commands. Macros often become the foundation for the more advanced customizations as they provide a good prototyping environment.

The VBA is a programming language for ArcGIS software and we can easily manipulate the ArcGIS ArcMAP functions and tools. With VBA, we can customize the way ArcMAP looks, modify ArcMAP's standard tools, create new tools, integrate ArcMAP with other applications and develop and distribute the custom applications on top of ArcMAP. In addition, VBA is convenient to use and its application to the lineament analysis for the ground water is very useful.

In this study, the main VBA script of "CalculateKForPolyline", "CalculateFractureDensity_LEN2", "CalculateFractureDensity_num" has been restructured and redeveloped for the lineament analysis and mapping. The first, "CalculateKForPolyline (calculate the orientation of the polyline)" is a script to calculate the lineament orientation. With this script, there is a finding in which direction the lineaments are oriented and they give us a clue of the ground water movements in the area and the place where the lineaments intersect to each other. The second and the third, "CalculateFractureDensity_LEN2 (Calculation of Lineament Length Density

value)" and "CalculateFractureDensity_num (Calculate Lineament number density)" are scripts to calculate the sum of the lineament length and the sum of lineament counts within the equi-spaced polygons or grid with a 5km wide respectively . With these data, the lineament density maps have been drawn. These density maps will be used for the analysis of the lineament with respect to the ground water occurrence.

The 3D Analyst Geoprocessing tools to create and modify raster surfaces, and then extract information and features from them. 3D Analyst toolsets let you convert features to raster, create 3D features from functional surfaces by extracting height information, interpolate information from raster, mathematically manipulate raster, reclassify raster, and derive height, slope, aspect, and volumetric information from raster.

One of the interpolation techniques is an IDW (Inverse Distance weight) interpolation which explicitly implements the assumption those things that are close to one another are more alike than those that are farther apart. To predict a value for any unmeasured location, IDW will use the measured values surrounding the prediction location. Those measured values closest to the prediction location will have more influence on the predicted value than those farther away.

During mapping of the lineament length density as well as the lineament number density, the polygons that represent each values of densities has been converted to points. The density values of each point are interpolated using the Inverse Distance Weight (IDW) in 3D analyst of ArcMAP to raster as seen in Figure 18 and 19. The lineament orientation map has been done by converting the lineaments in point feature and those points are interpolated using IDW in to raster as seen in Figure 21.

CHAPTER THREE

Results and Discussion

3.1. Thermal mapping

3.1.1. Radiance

The result of the thermal infrared image of the high gain and low gain in which converted to the radiance with that of histogram are as shown in Figure 9-a and Figure 9-b respectively. The radiance computed for low gain ranges from 4.9228 to 8.948 with mean 6.991 and standard deviation 0.826. For that of high gain it ranges from 7.9126 to 11.261 with a mean of 9.647 and standard deviation 0.692.

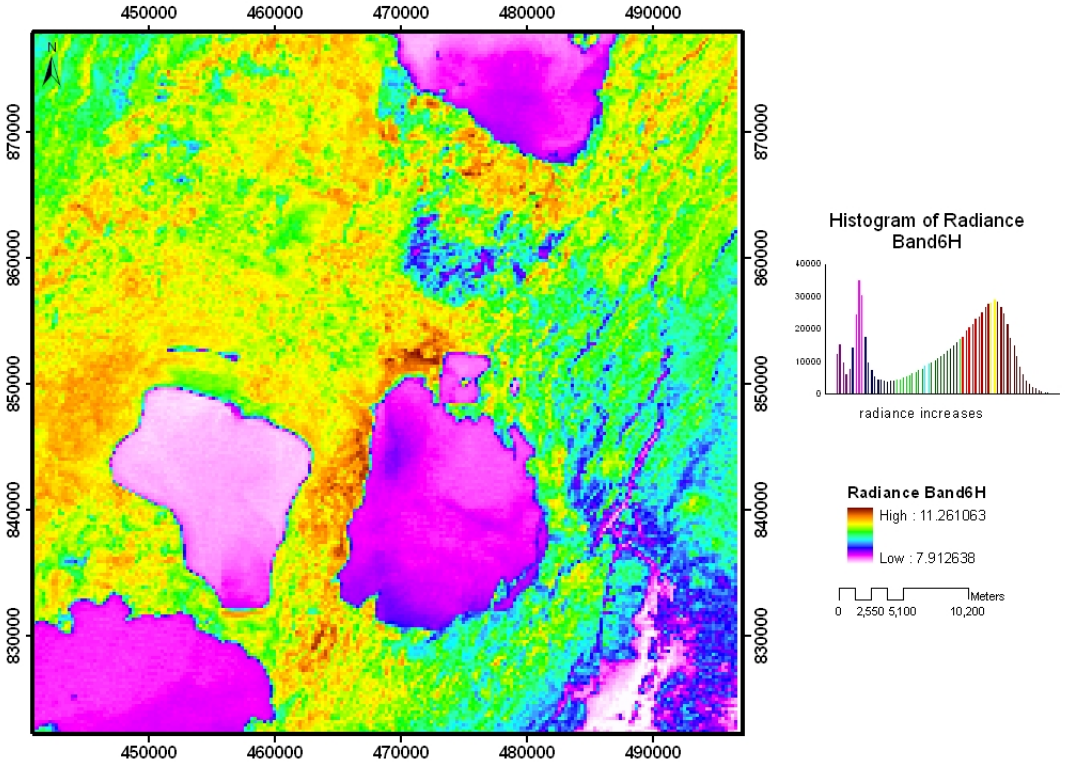

Figure 9-a: Radiance and histogram of thermal band high gain image

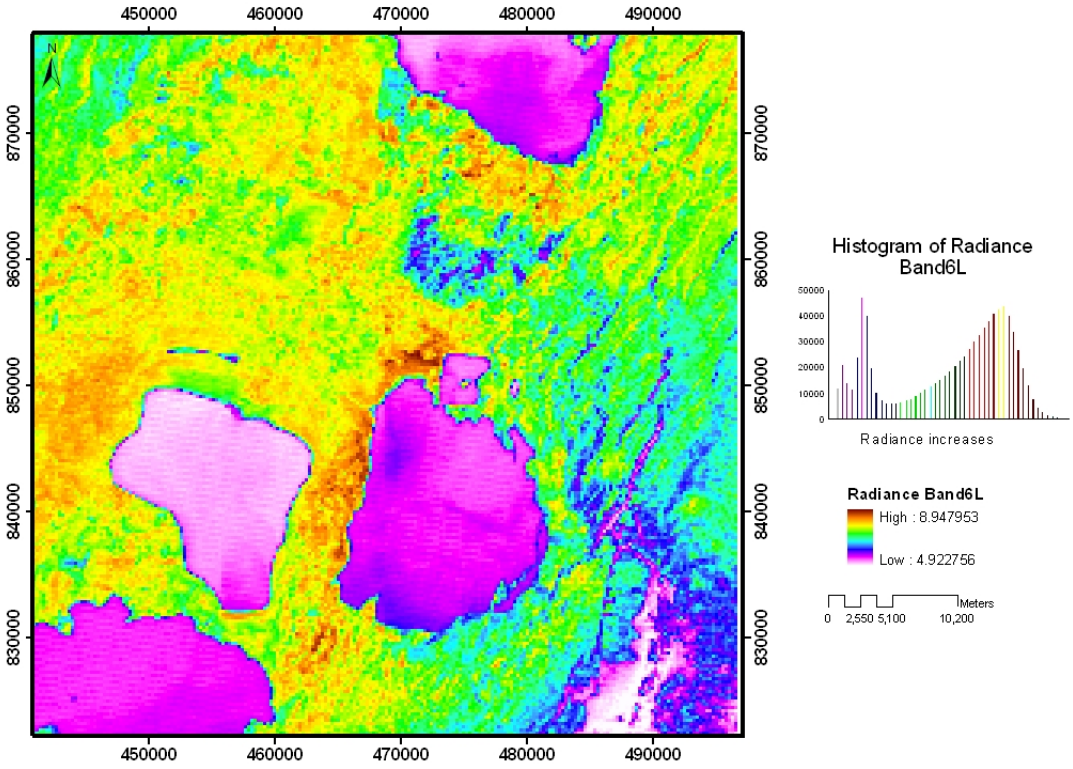

Figure 9-b: Radiance and histogram of thermal band low gain image

3.1.2. At Satellite temperature

The result of the radiance image of the high gain and low gain in which converted to the at_satellite temperature (Appendix 5-1) with the histogram is shown in Figure 10-a and Figure 10-b respectively. The at_satellite temperature ranges from 288 to 312 with a mean of 300.965 and standard deviation 5.061 for the high gain thermal band Figure 10-a and from 260 to 296 with a mean of 279.761 and standard deviation 7.363 for the low gain thermal band Figure 10-b.

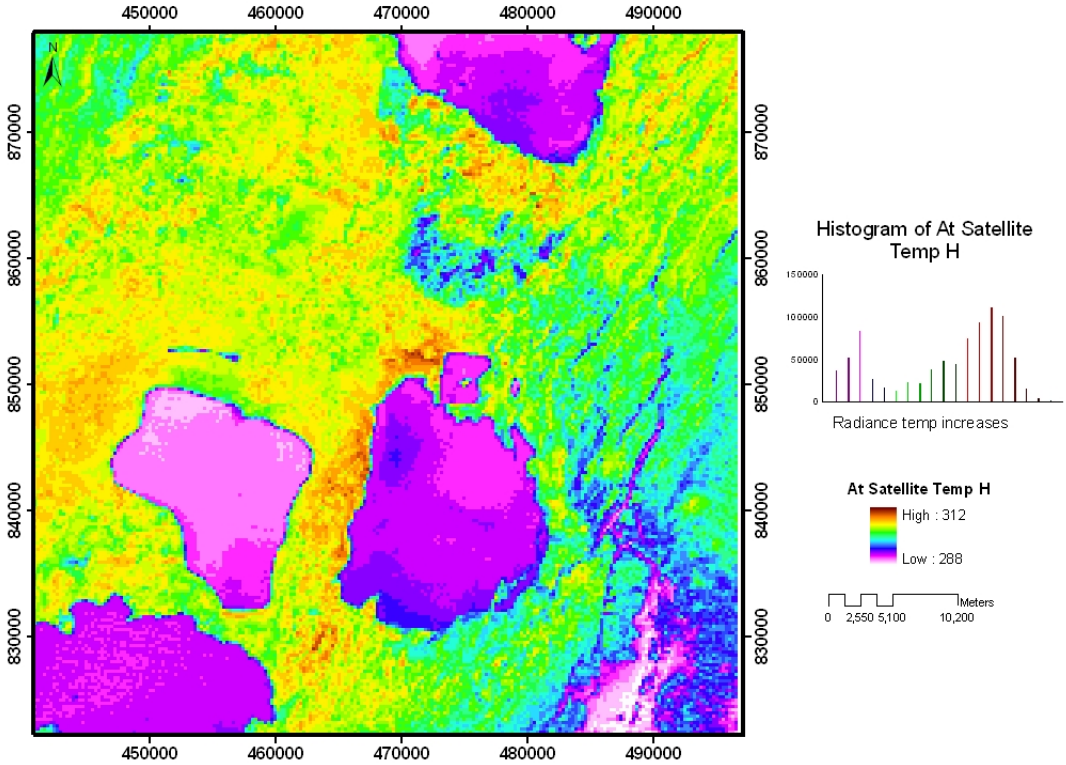

Figure 10-a: At satellite temperature and its histogram for thermal band 6 high gain

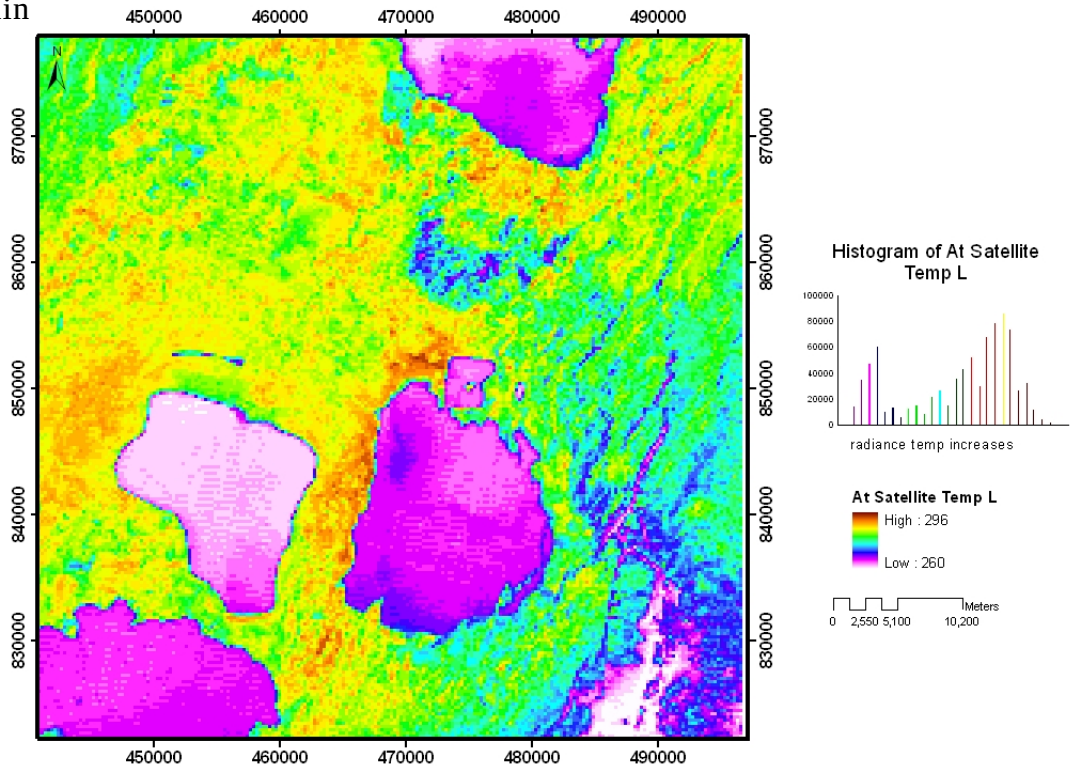

Figure 10-b: At satellite temperature and its histogram for thermal band 6 low gain

3.1.3. Emmisivity Corrected at_satellite temperature

The efficiency that an object radiates energy that is the emissivity for LANDSAT 7 is estimated using Van griend and Owe method from Normalized difference in vegetation index (NDVI) in Figure 11. The emissivity computed for LANDSAT 7 ranges from 0.9229 to 0.9831 with the average 0.9460 (Figure 12). The highest emissivity is shown in areas where there is dense vegetation.

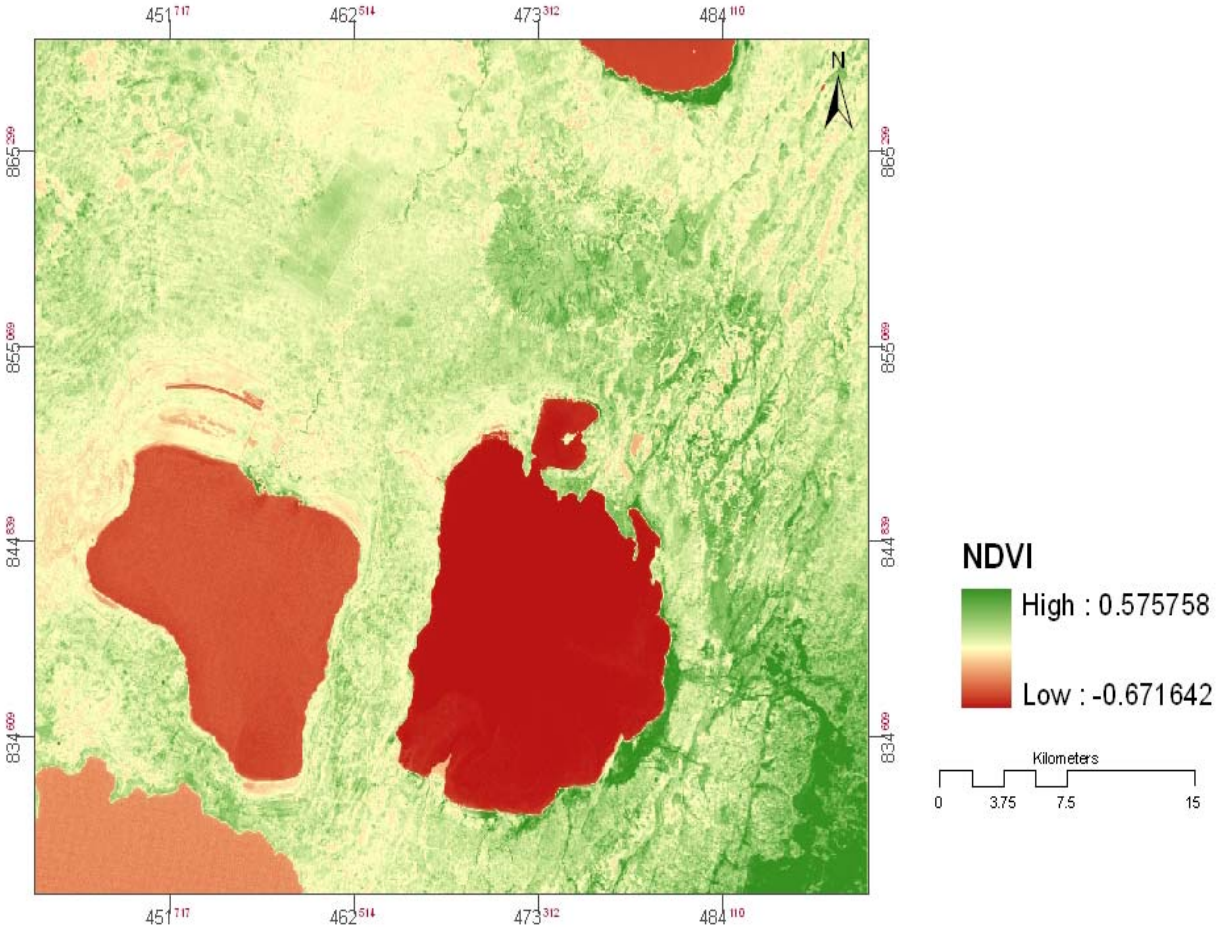

Figure 11: Normalized Difference Vegetative Index for the LANDSAT 7 image.

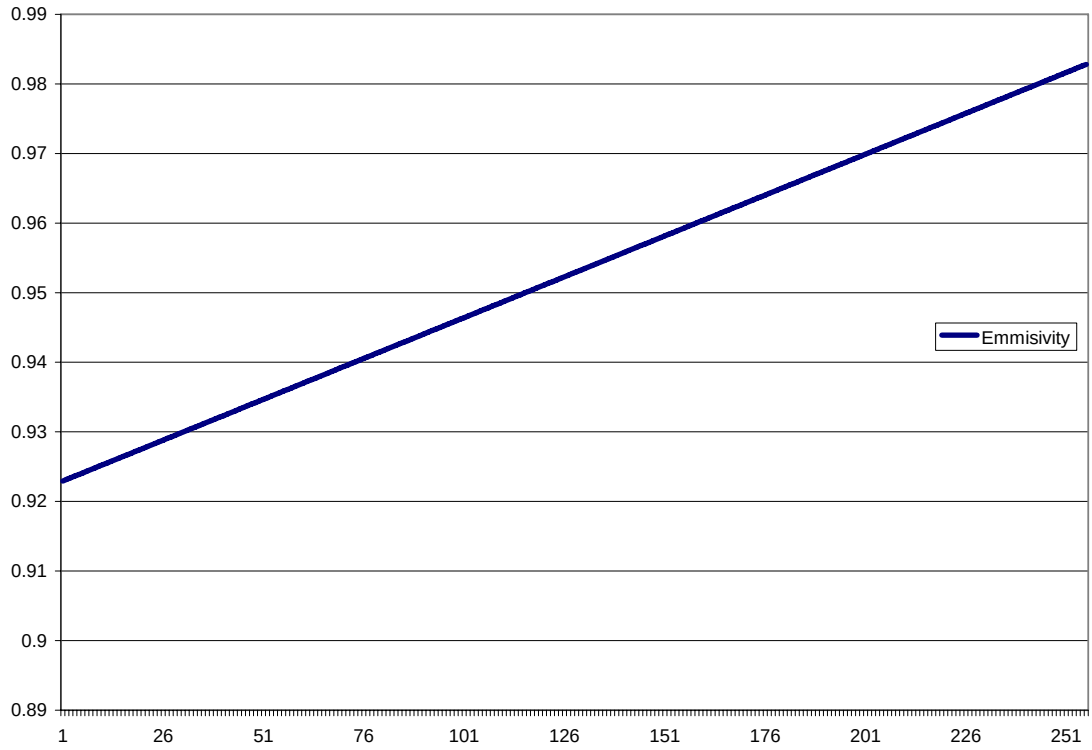

Figure 12: Graph of the emmisivity for LANDSAT 7 ETM+

The result of at satellite temperature image of the high gain and low gain in which converted to the emmisivity corrected at satellite temperature (Appendix 5-2) and the histogram is shown in Figure 13-a and Figure 13-b respectively. The emmisivity corrected at satellite temperature ranges from 285 to 308 with a mean of 297.53 and standard deviation 4.683 for the high gain thermal band and from 257 to 293 with a mean of 276.761 and standard deviation 7.363 for the low gain thermal band.

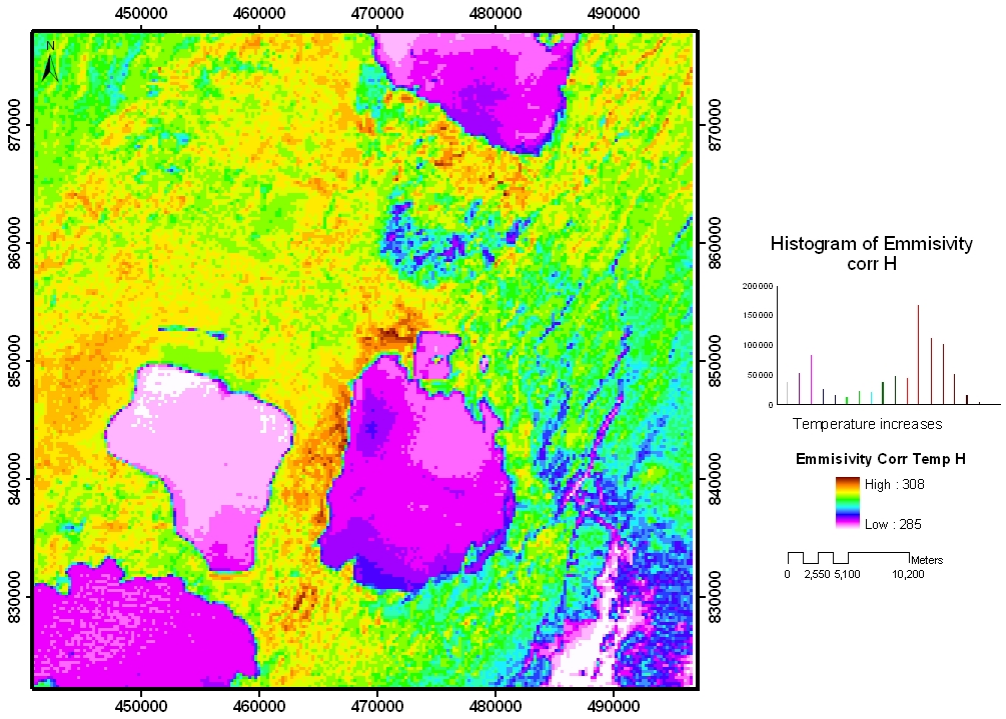

Figure 13-a: Emmisivity corrected at satellite temperature and its histogram for LANDSAT 7 band6H.

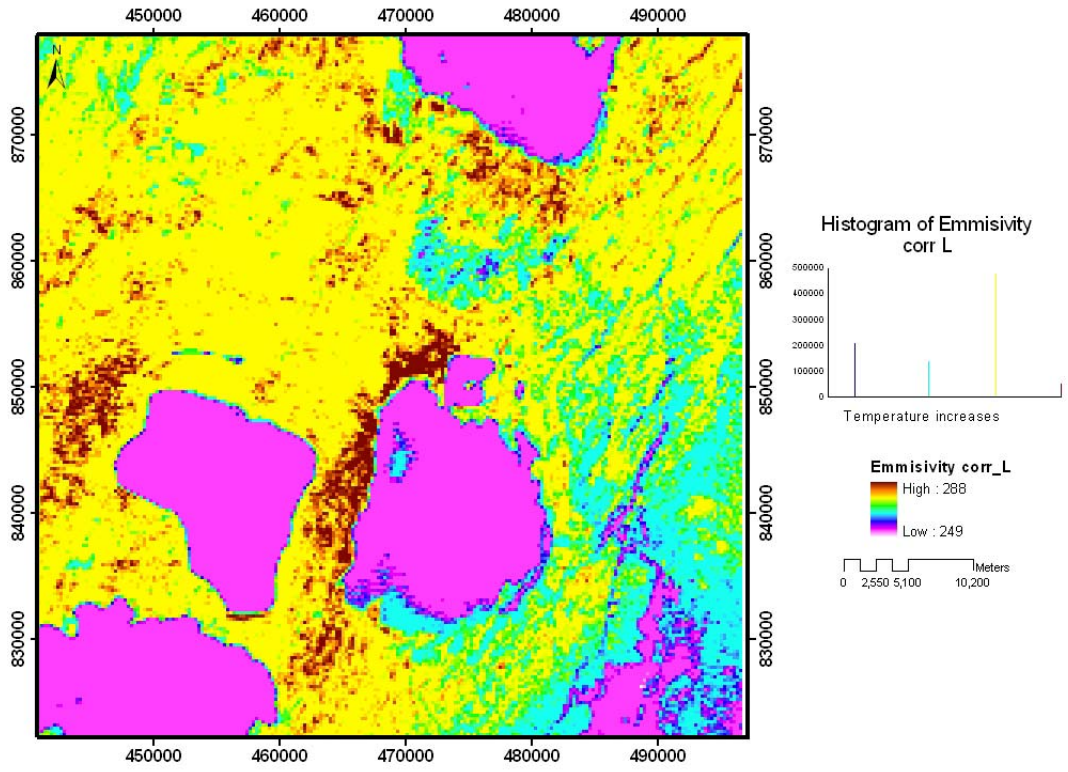

Figure 13-b: Emmisivity corrected at satellite temperature and its histogram for LANDSAT 7 band6L.

3.1.4. Surface Kinetic Temperature

The surface kinetic temperature is computed using the equation 5 and the script is done in ERDAS imagine software as shown in appendix 5-3. Figure 14-a and 14-b show the distribution of land surface kinetic temperature values of Langano and Abijata lakes region for band 6 high gain and low gain respectively. Using the low gain Figure 14-b, the Kinetic temperature ranges from 259 to 296 with a mean of 278.761 and standard deviation 7.363. Using the low gain Figure 10-a, the Kinetic temperature ranges from 287 to 311 with a mean of 300.285 and standard deviation 5.065. Both the kinetic temperature of low gain and high gain are overlaid using ERDAS imagine software and it gives a result of shown in Figure 15 which has a maximum value 311, minimum value 287, mean of 300.285 and standard deviation 5.065.

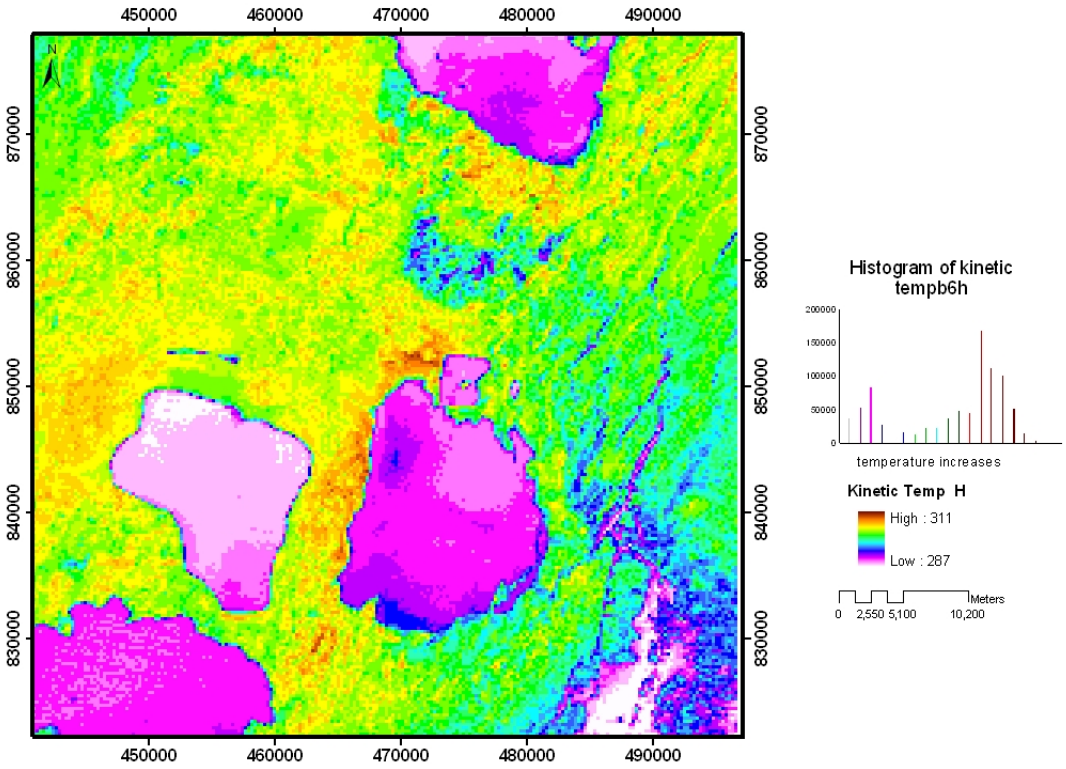

Figure 14-a: Surface kinetic temperature and its histogram for LANDSAT 7 band6H.

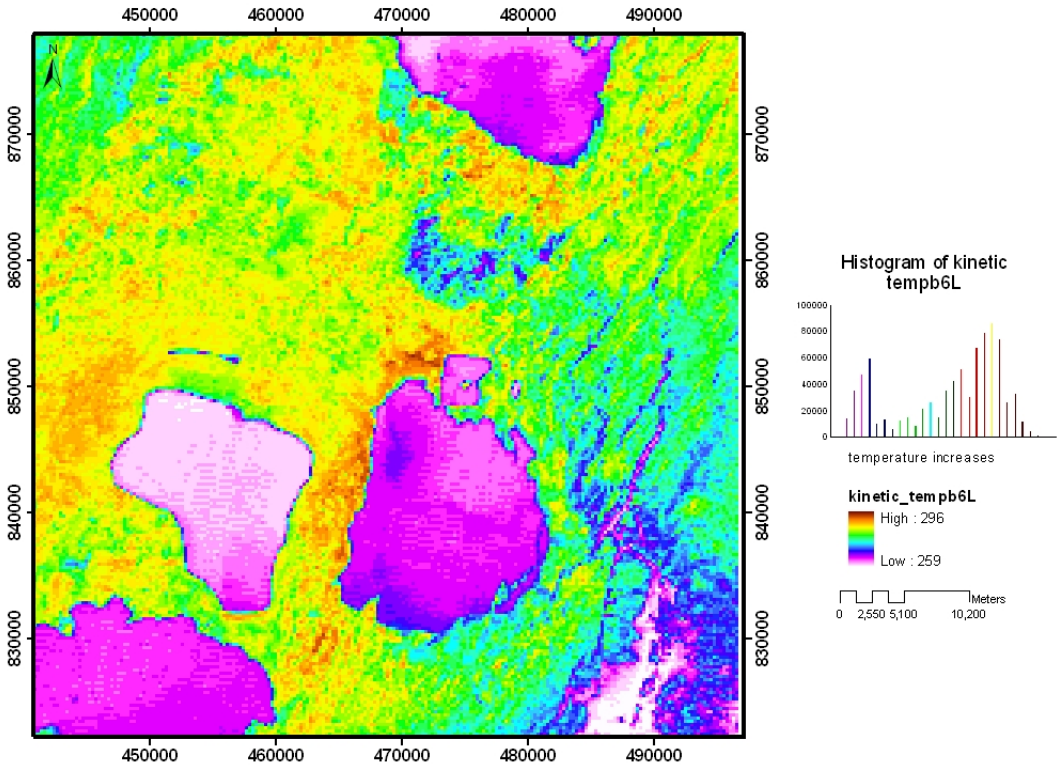

Figure 14-b: Surface Kinetic temperature and its histogram for LANDSAT 7 band6L.

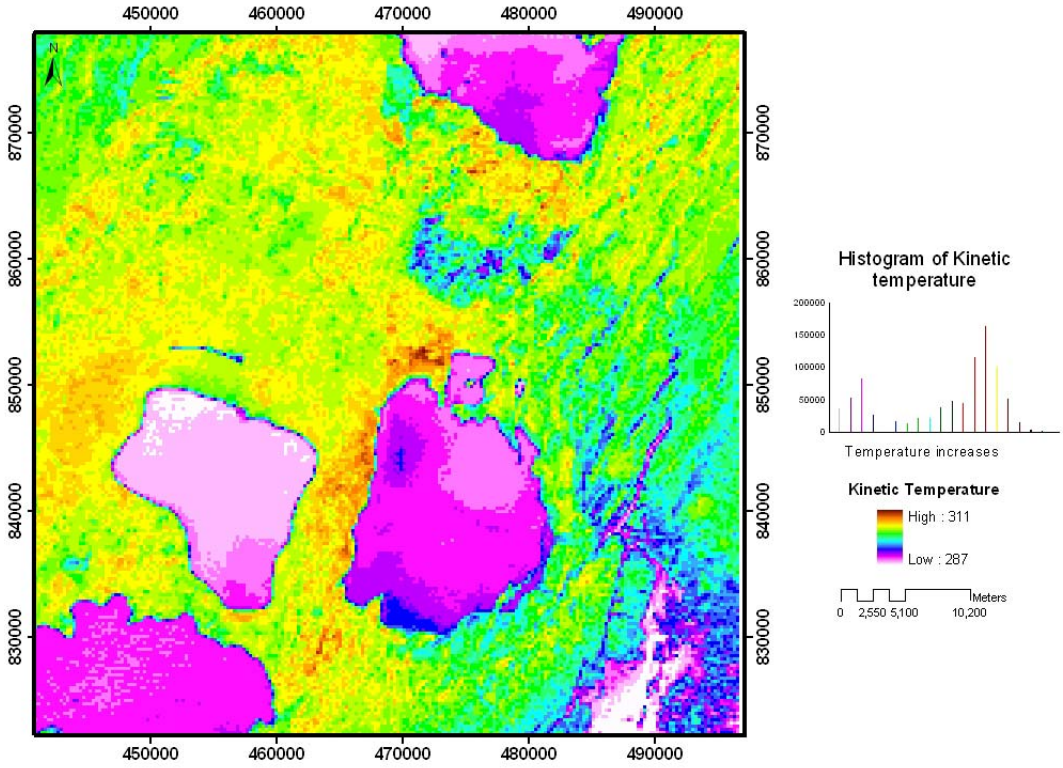

Figure 15: The colored combined image of kinetic surface temperature

Even if Interpreting thermal data and images of temperature distribution over an area is not often an easy job, since each component surface in the landscape exhibits a unique radiative, thermal, moisture and other properties, and relates to their surroundings site environment, it is evident from the map that there is a thermal gradient as progressed from the floor of the rift to the high lands. Some hot spots or high thermal manifestation areas can be easily identified. The most extensive thermal manifestation is around the bottom of the Aluto mountain area and near the Langano Lake at the north shore. There are also many smaller thermal exhibited areas along the west Shore of Langano Lake and Abijata Lake. How ever, there did not an extensive thermal manifestation in the eastern part of Lake Langano, except for a few small ones along the North eastern shore of Lake Langano.

3.2. Lineament Analysis

3.1.1. Preparation of basic Lineament map

Lineaments have been screen digitized from the existing 1:500,000 scale structural map of the main Ethiopian rift (Bekele et., al.,2000) and additional lineaments extracted from the LANDSAT ETM+ image using spatial filtering and edge enhancement technique in ERDAS software.

After using the high pass directional filtering technique, the following images have been carried out and using those resulted images additional lineaments extracted (Figure 16 and 17)

1	0	1
2	0	2
1	0	1

A) North-South Kernel

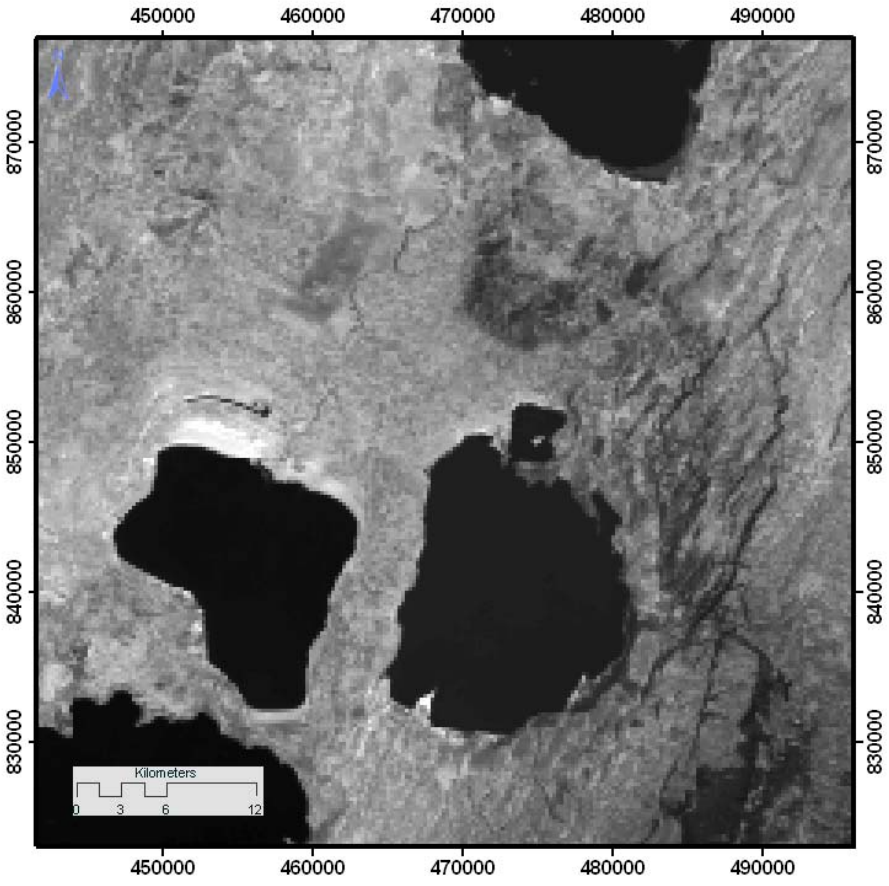

-1	-2	-1
0	0	0
1	2	1

B) East-West Kernel

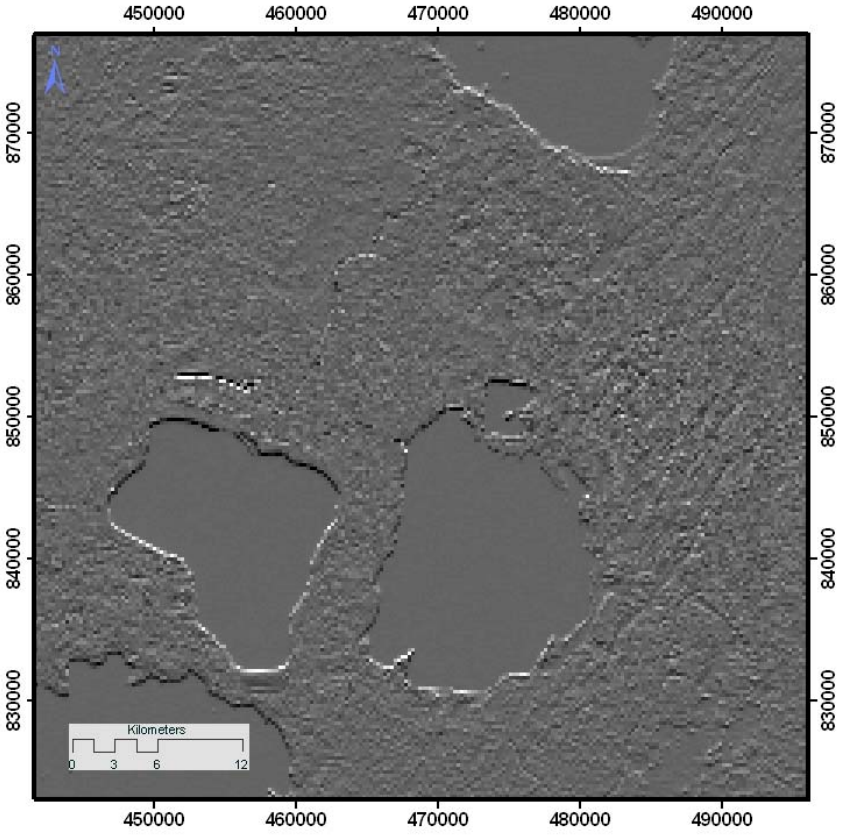

2	-1	0
-1	0	1
0	1	2

C) NorthEast-SouthWest Kernel

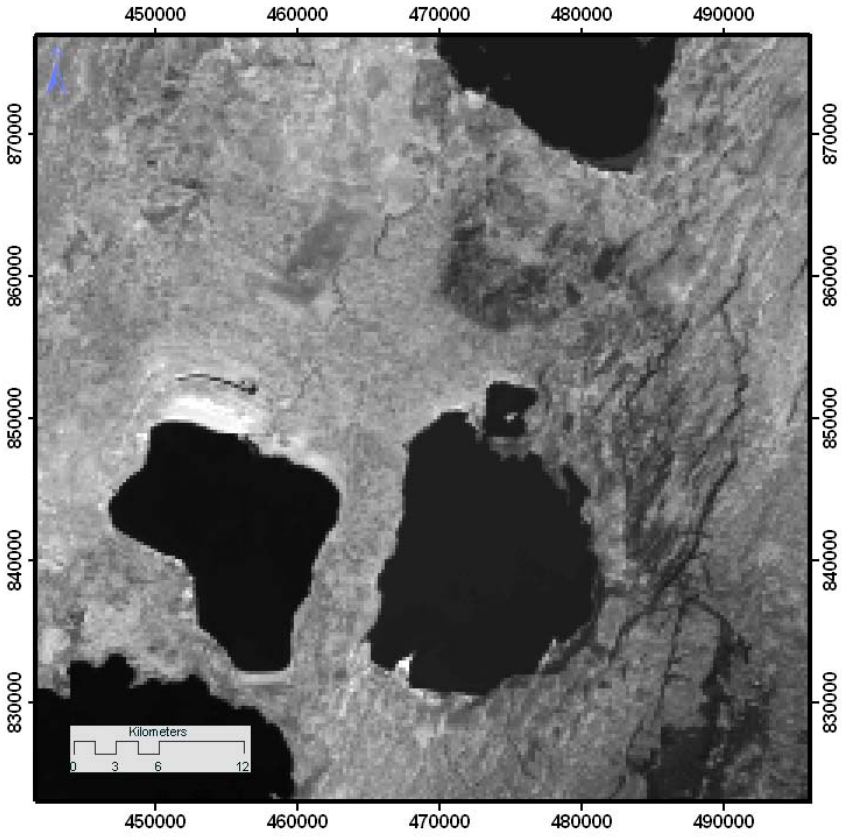

0	-1	-2
1	0	-1
2	1	0

D) NorthWest-SouthEast Kernel

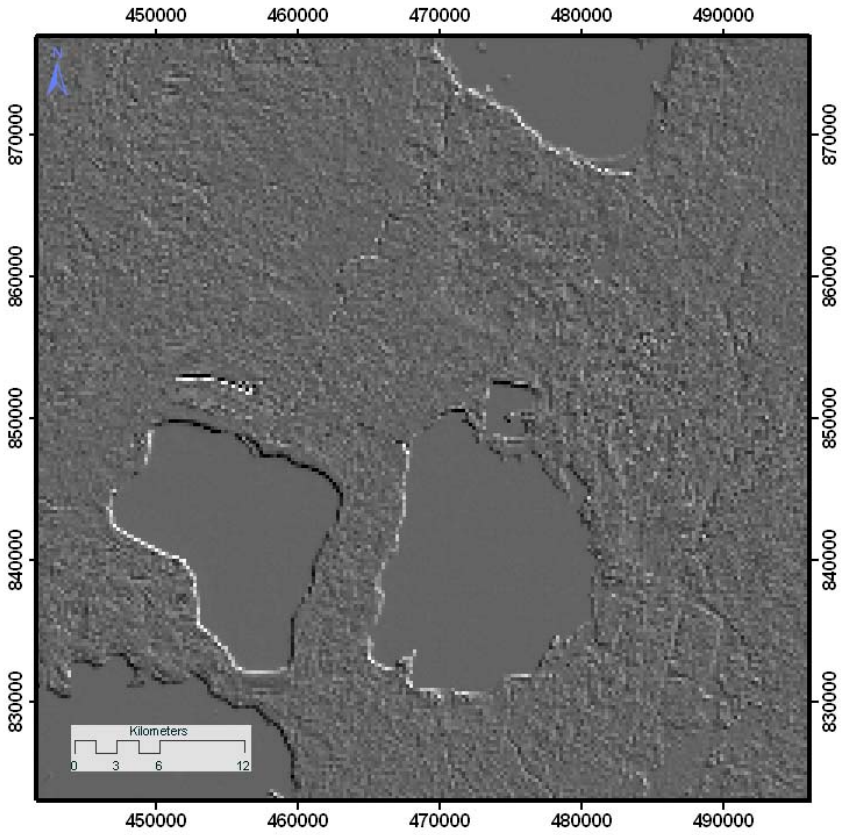

Figure 16: the filtered images using spatial filtering A) using North-South Kernel and the filtered image B) East-West Kernel and its result C)NorthEast-SouthWest Kernel and filtered output D)NorthWest-SouthEast Kernel and its result

The above filtered images are mosaiced using ArcGIS 9.1 Software by taking the maximum values and resulted as shown below. And additional lineaments have been extracted by tracing the lineaments using the four directional filtering techniques with a scale of 1:100000. These lineaments are added to the lineament analysis using VBA.

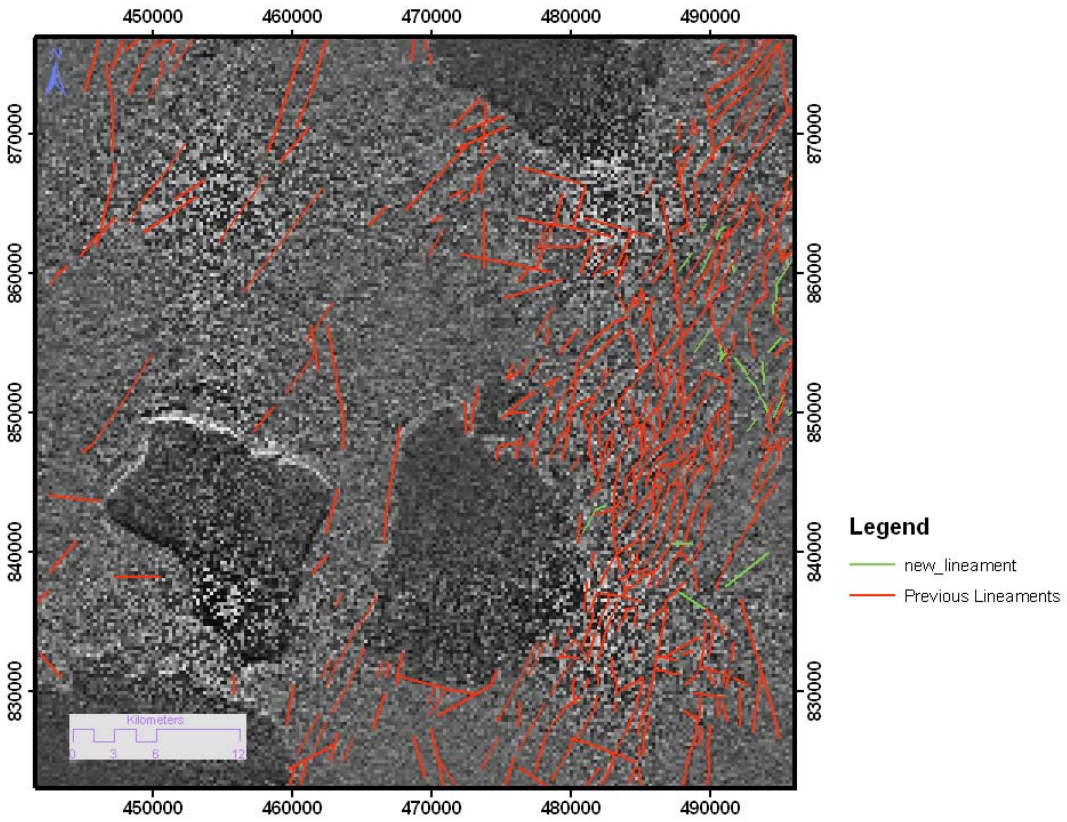

Figure 17: Extracted lineaments from the four directional filtered images with a scale of 1:100000

The extracted lineaments for the specific area of interest in combination with the digitized lineaments as shown in the Figure 7 have been used as a lineament feature that appears as a second layer in ArcMAP of ArcGIS 9.1 software for the lineament analysis and the study area image is converted to grids of equal size with a 5km width (Figure 8) which appears as a first layer in the ArcMAP.

Then after lineament length density, lineament number density and lineament orientation programs have been developed. Using the programs lineament length density, lineament number density and lineament orientation maps has been carried out. These out put maps are further analyzed with respect to ground water occurrence.

3.1.2. Lineament Length density

A script “CalculateFractureDensity_LEN2” computes lineament length density value using VBA language. It calculate first the sum total of the lineaments in each grid or polygons that have been created from the image and then the lineament length density values are computed using the script file (Appendix 2). The out put of the script file is stored on the attribute table of the polygon feature class of field name “DENS_LEN” as shown in table 8. After calculating this density value a lineament length density map (Figure 18) is constructed based on the computed values using ArcGIS ArcMAP program. As you observe on the lineament length density map, the density is more on the eastern part of Lake Langano and mountain Aluto, blue in color, compared to the floor of the rift, orange in color. And it is even declines in density when it goes from the high lands to the rift floor.

ID	GRIDCODE	Dens_num	F_AREA	Dens_len
1	117	0.208	25000000.000	757.904
2	125	0.108	25000000.000	952.824
3	100	0.220	25000000.000	527.600
4	87	0.000	25000000.000	0.000
5	91	0.000	25000000.000	0.000
6	88	0.000	25000000.000	0.000
7	120	0.368	25000000.000	921.660
8	119	0.968	25000000.000	2470.920
9	113	0.000	25000000.000	0.000
10	115	0.172	75000000.000	869.621
11	118	0.060	25000000.000	430.140
….	…..	…..	……	…..
….	….	….	…..	…..
95	114	0.320	25000000.000	605.040
96	112	0.660	25000000.000	1817.240
97	101	0.616	25000000.000	2256.616
98	89	0.220	25000000.000	718.120
99	98	0.208	25000000.000	782.912

Table 8: Table structure and an example of output file produced by “CalculateFractureDensity_LEN2” and “CalculateFractureDensity_num” scripts

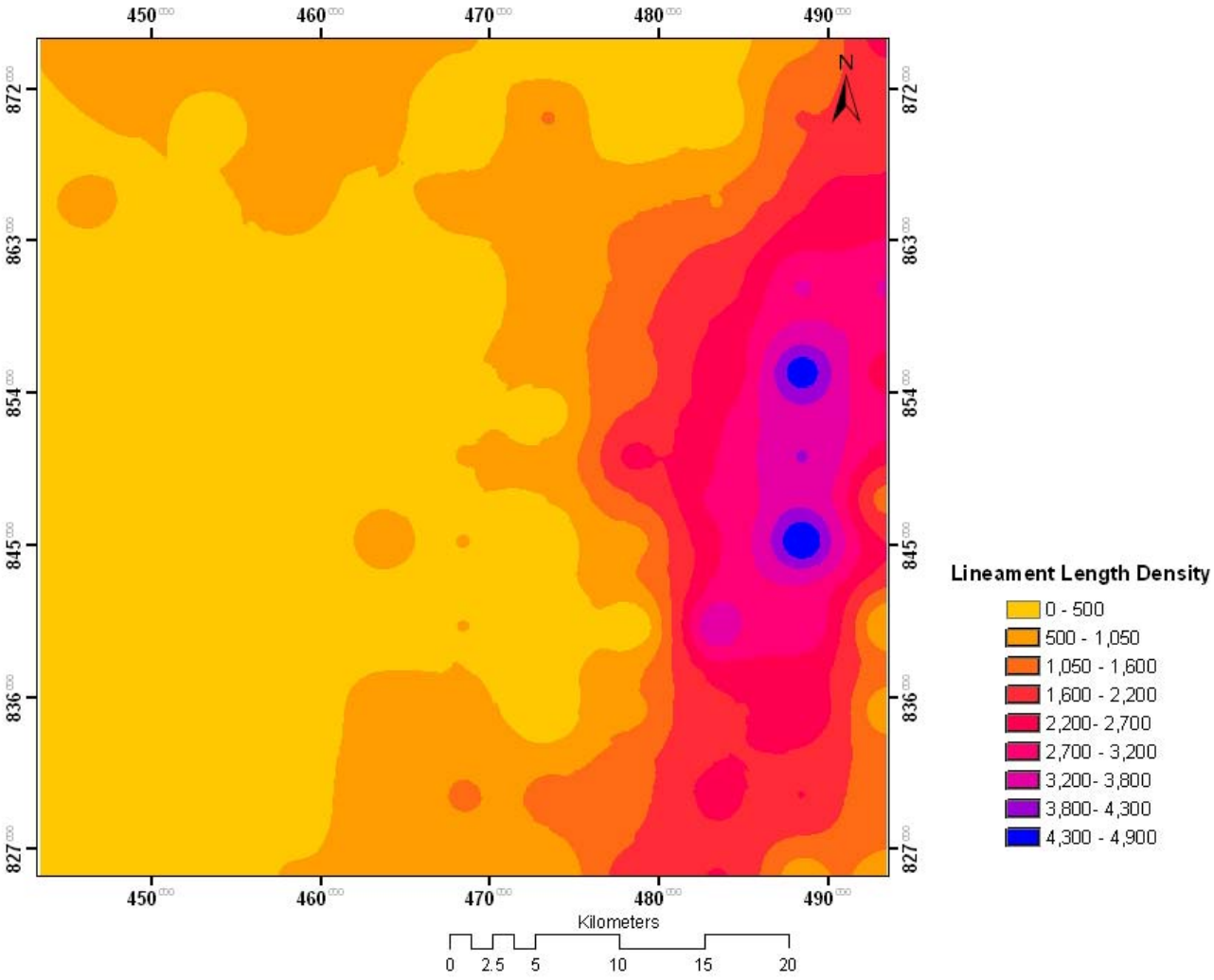

Figure 18: Lineament length density map constructed using the result of script (Appendix 2)

3.1.3. Lineament Number density

A script "CalculateFractureDensity_num" computes lineament Number density value is developed using VBA language. When constructing lineament density map the script counts Lineaments with in each grid or polygons that have been created from the image and calculates lineament number density values (Appendix 3). The out put of the script file is stored on the attribute table of the polygon feature class in the field name called "DENS_NUM" as shown in table 8 After calculating this density value a lineament Number density map

(Figure19) is constructed based on the computed values using ArcGIS ArcMAP program. In the map, the blue colored areas are the most densely areas which exhibit 1.33 – 1.5 and the yellowish orange color is sparsely populated area which is in between 1- 0.16. And when we compared with that of the lineament length density map, this map shows high density to the west side of the Aluto Mountain which is southwards the lake Ziway.

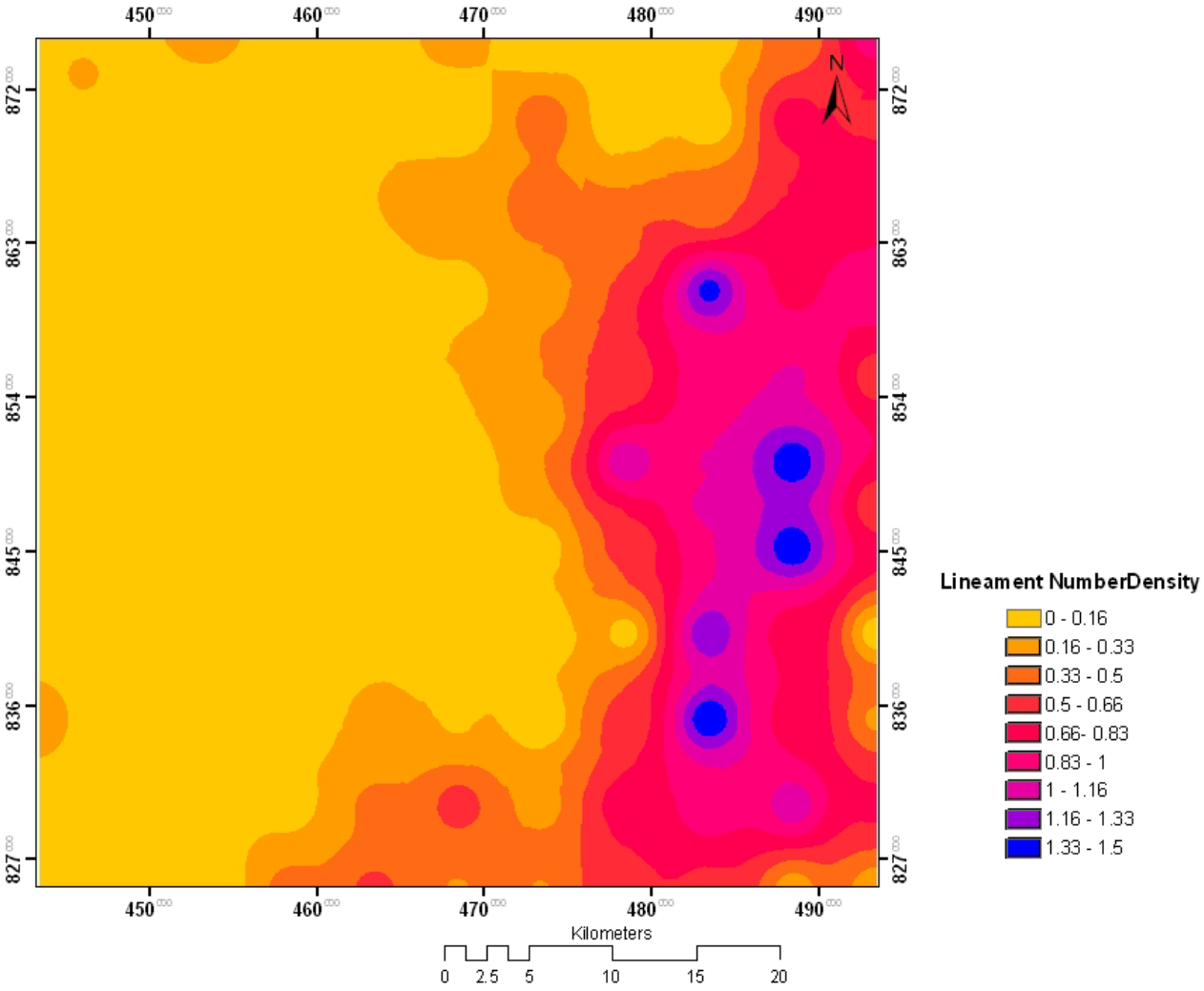

Figure 19: Lineament Number density map constructed using the result of script (Appendix 3)

The lineaments are classified in to three categories

1. High density
2. Medium density
3. low density

The high density in number as well as in length area is located on the east side of lake Langano and east side of Aluto mountain and the density decreases away from the escarpment towards west side of the lake Langano and Aluto mountain which is the floor of the rift valley.

3.1.4. Lineament Orientation

A script "CalculateKForPolyline" computes lineament orientation value is developed using VBA language in ArcMAP. This script calculates the lineament orientation and number of nodes of lineaments that are present in the lakes region of the Ethiopian Rift valley (Appendix 3). The out put of the script file is stored on the attribute table of the Lineament feature class in the field name called "ORIENT" and "NUM_PNTS" as shown in table 9. After calculating this Lineament orientation, a lineament orientation map and a rose diagram that shows the general trend of the lineaments (Figure 20) are constructed based on the computed values using ArcGIS ArcMAP program.

No	SHAPE_LENGTH	ORIENT	ORDER_NO	NUMPNTS
1	15969	68.965	1	25
2	9453	76.751	1	20
3	11475	66.191	1	20
4	11672	66.679	1	18
5	9104	60.148	1	18
6	10816	55.830	1	18
7	7616	66.930	2	17
8	11735	64.032	1	16
9	7036	60.040	2	16
10	9369	63.475	1	15
11	6532	61.044	2	13
12	4560	50.268	3	13
13	5019	-19.904	2	13
…	….	…	….	….
…	…	….	….	….
327	2806	-84.806	3	2
328	1248	-86.186	3	2
329	1913	-87.508	3	2
330	523	-89.186	3	2

Table 9: table structure and an example of output file produced by "CalculateKForPolyline" script

The orientation of the lineaments classified in to two based on their orientation.

1. Between -90^{o} (west) to 0 (North), blue in color on the map.
2. Between 90^{o} (East) to 0(North), orange in color on the map.

Most of the lineaments in the study area are oriented NE-SW direction as shown in the Figure 20 and in the rose diagram. And there are lineaments oriented to NW-SE direction in which they cross the NE-SW oriented lineaments. From the map, the boundaries between the NE-SW trending and NW-SE trending lineaments tell us the cross over of those lineaments around that area. In addition, from the rose diagram most lineaments are even oriented in the direction of ENE-WSW rather than the other directions.

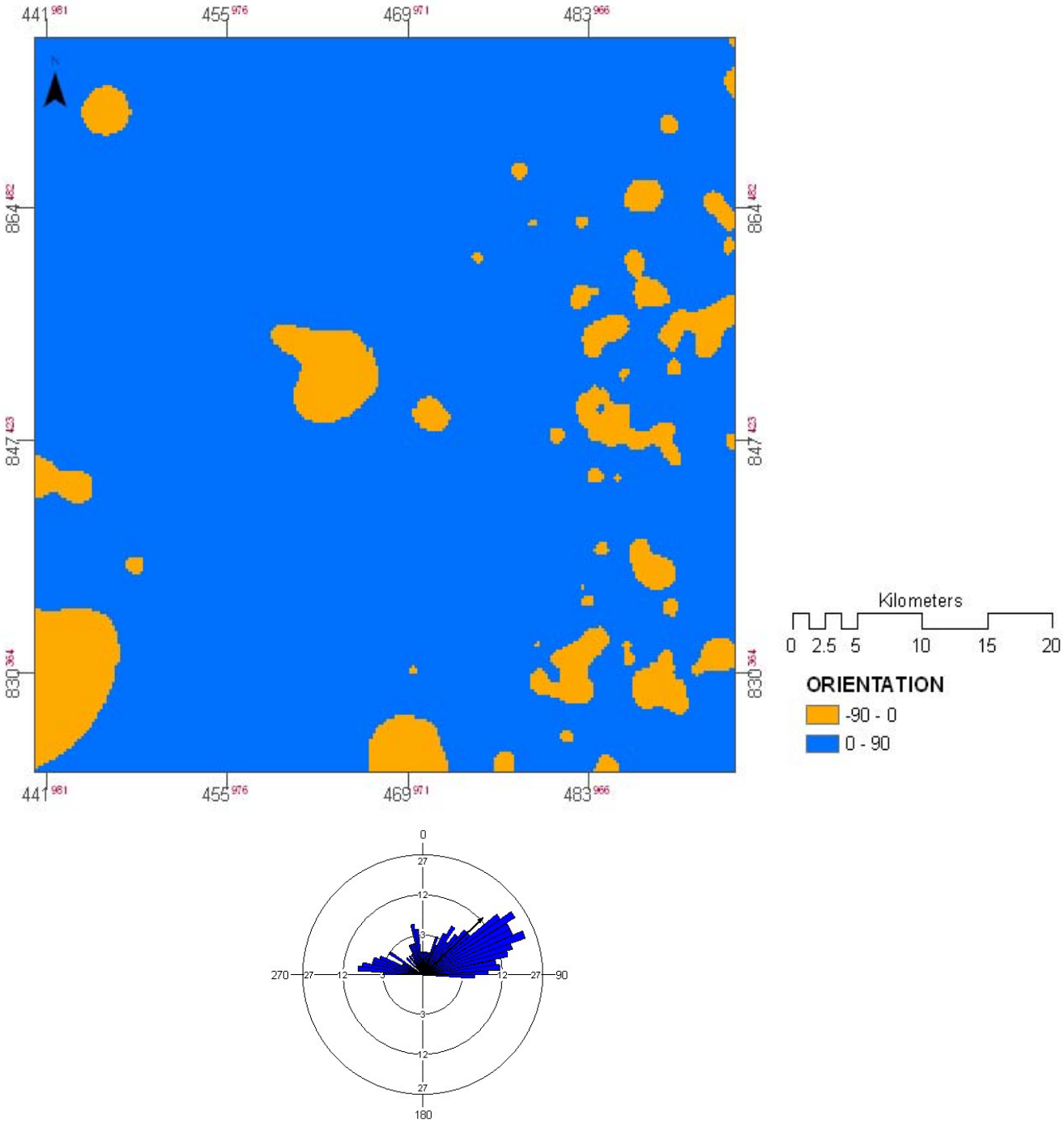

Figure 20: Lineament Orientation map and rose diagram constructed using the result of script (Appendix 3)

3.1.5. Lineaments with Ground water occurrence

Fractures zones characterized by high transmissivity generally generate the high groundwater production area but it is very probabilistic to identify these highly productive fractures. Structural analysis, chemical analysis and tectonic history study can provide useful information for this problem in regional scale studies.

In this study, partly in the lineament analysis, the cross over and the density of the lineaments are clearly observed from the orientation map and the lineament density maps. When the orientation maps and density maps related to the groundwater flow (Figure 21 and 22), the lineaments act as a conduits for the movement of groundwater close to the escarpment because the decline of the density as well as the cross over of the lineaments coincide with the flow of the groundwater. This is also confirmed (Figure 23) from the groundwater table contour, the contour values decrease from the escarpment to the floor of the rift by reflecting the flow direction. This is good witness for conduit characters of highly dense lineaments.

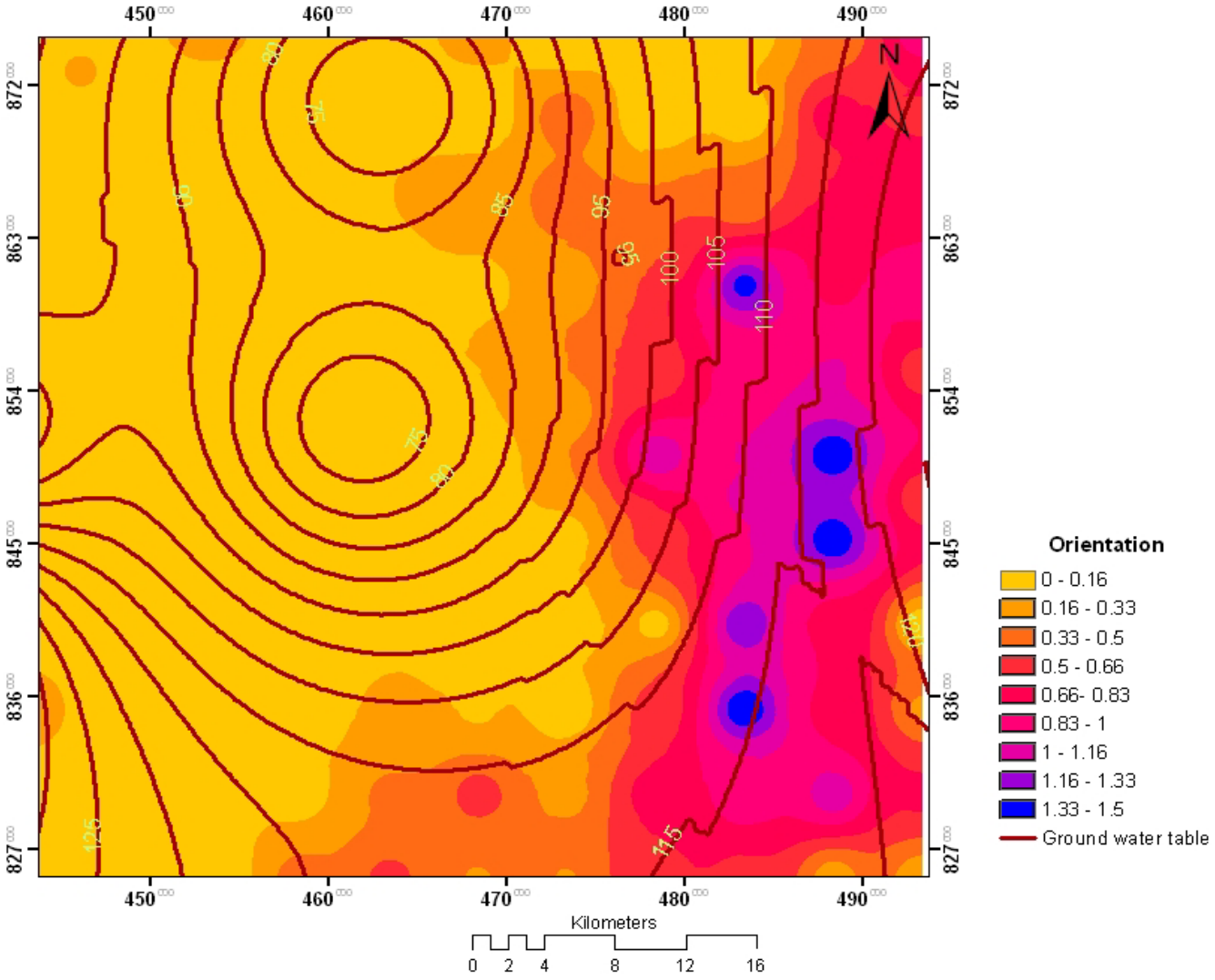

Figure 21: Lineament density map is overlaid with the ground water table contour.

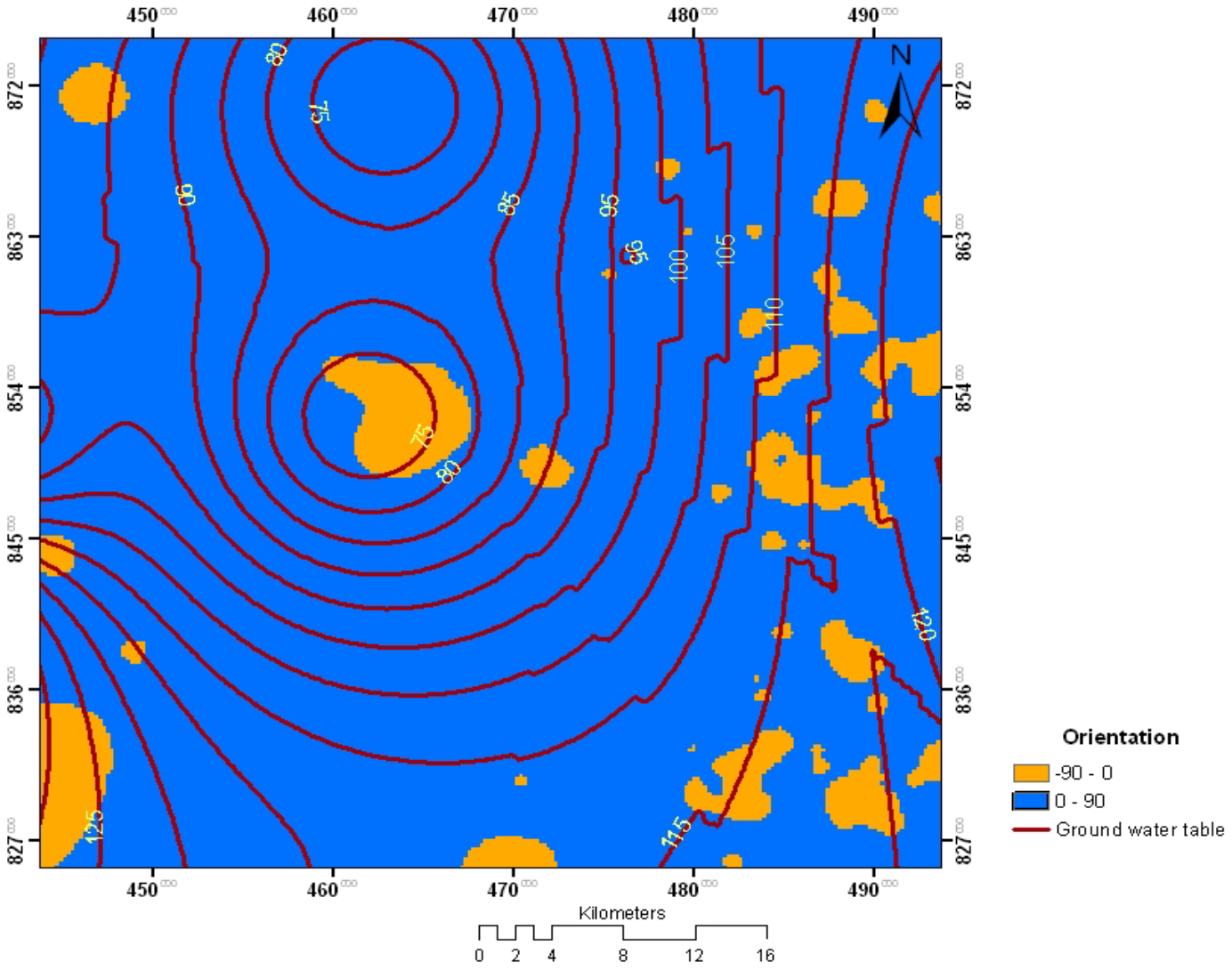

Figure 22: Lineament orientation map is overlaid with the ground water table contour.

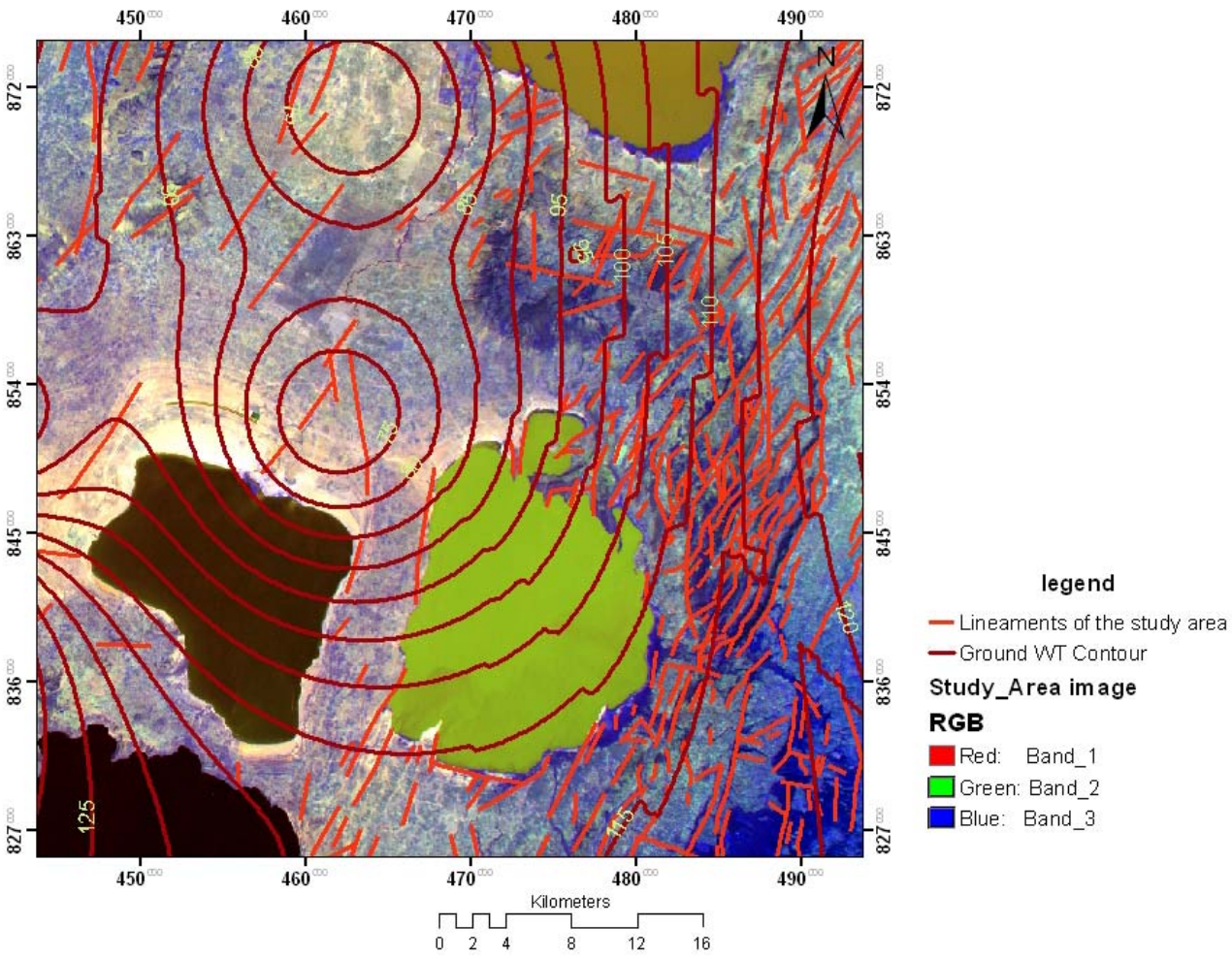

Figure 23: Map of Lineaments in the study area is overlaid with the ground water table contour.

In this study, a comparison of Lineaments with that of groundwater chemistry has been done for determination of the relationship of the lineaments with occurrence of groundwater.

From the study area Shimelis compiled water sample data from 317 wells. The distribution of the wells is shown in Figure 24. He grouped the water from the wells into seven sub-groups based on their chemistry. These wells are distributed in each sub group, which have been identified and named using

HCA (Table 10: shimelis, 2006). From these, 14 of them are within sub group 2, 6 of them are within the sub group 5, 6 of them are in sub group 3, 5 of them are with in sub group 1, 3 are in sub group 6, 3 are with in the sub group 4 and 3 are in sub group 7 (Appendix 4). The mean values of ions in each well in the Ziway-Shala basin are summarized in table 10. Sub groups 5 and 6 show relatively high TDS values, which confirmed that, there is water migration from other eastern part of the study area to these drilled wells. Sub group 4 representing the floor of the rift and characterized by highest TDS and Cl which could also be a good conformation for the flow of groundwater direction. The presence of group 1 and 2 wells in the study area, which have low TDS, might indicate that there is an interaction of the ground water to the lake water.

Generally, as confirmed in the above, the groundwater flows from eastern part of the study area to the floor of the rift and in turn the concentration of the lineaments relatively high in the eastern part which may encouraging the fast circulation of groundwater in this part.

Group	Sub_Group	Ca	Mg	Na	K	CO3	HCO3	Cl	SO4	TDS
Group_A	Sub_Group1	0.98	0.42	1.55	0.25	0.15	3.35	0.44	0.08	332
Group_A	Sub_Group2	0.43	0.26	3.86	0.31	0.07	4.57	0.49	0.09	475
Group_A	Sub_Group3	0.14	0.06	15.61	1.37	0.65	11.78	2.46	0.13	1184
Group_B	Sub_Group4	0.03	0.03	97.51	1.02	6.74	44.48	38.75	0.7	6538
Group_B	Sub_Group5	0.06	0.03	40.88	2.05	0.12	25.91	13.16	0.76	3351
Group_B	Sub_Group6	0.07	0.15	43.6	4.31	1.08	22.18	13.09	3.71	3249
Group_B	Sub_Group7	0.06	0.02	28.27	1.11	0.26	21.47	2.48	2.99	2441

Table 10: Mean values (unit in meq/l) for groups and subgroups derived from Hierarchical cluster analysis (HCA) (Shimelis, 2006) TDS is in mg/l

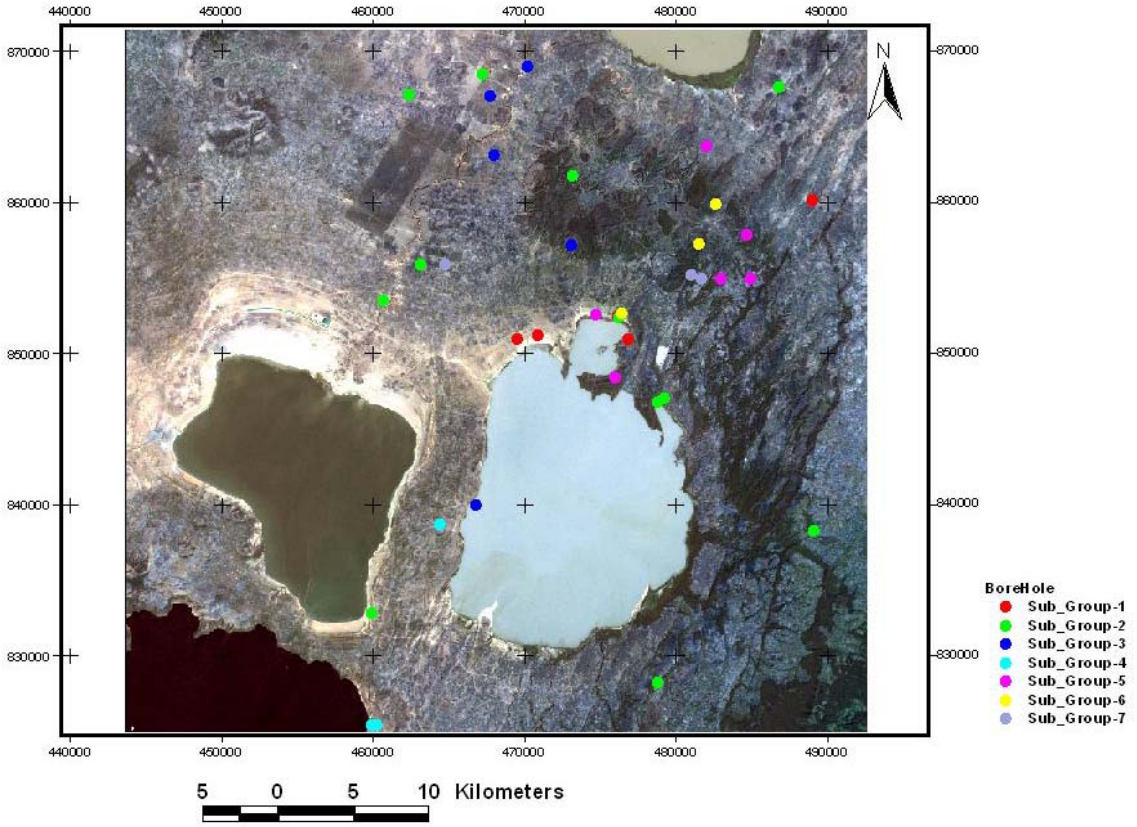

Figure 24: well distribution and their perspective subgroup

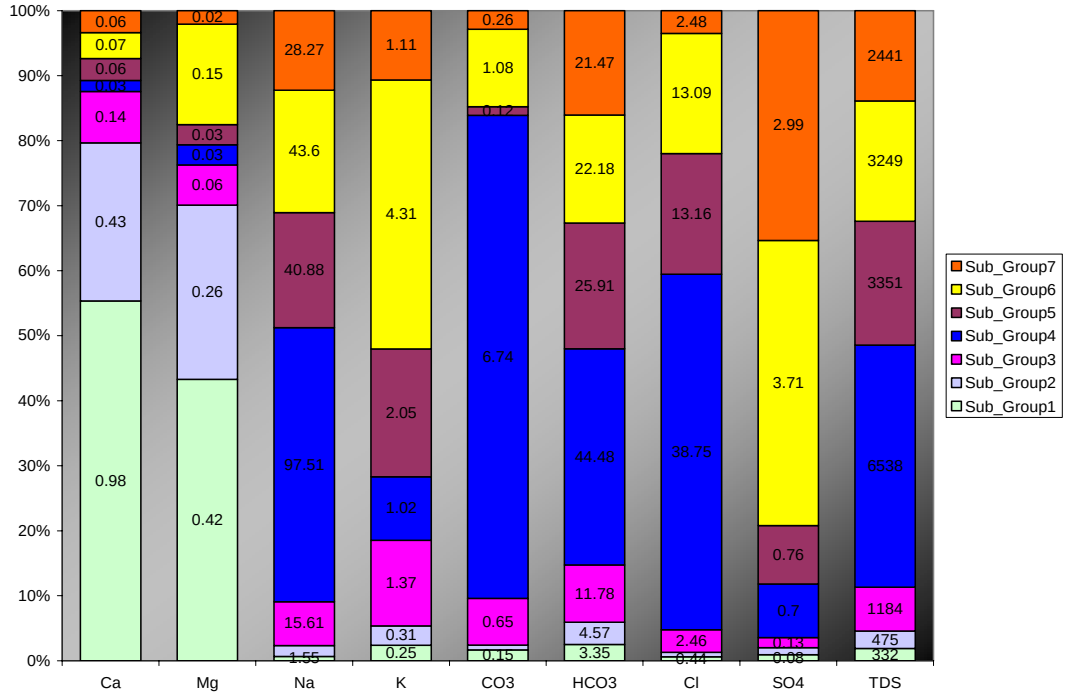

Figure 25: Collins bar diagram using subgroup mean defined by HCA

3.2. Comparison of Lineaments and Thermal manifestation

In the case of comparison analysis Figure 26 is constructed. This has been done by overlaying the lineaments with that of the thermal map in Arc GIS 9.1. From the Figure most the lineaments are found on the thermally anomalous areas.

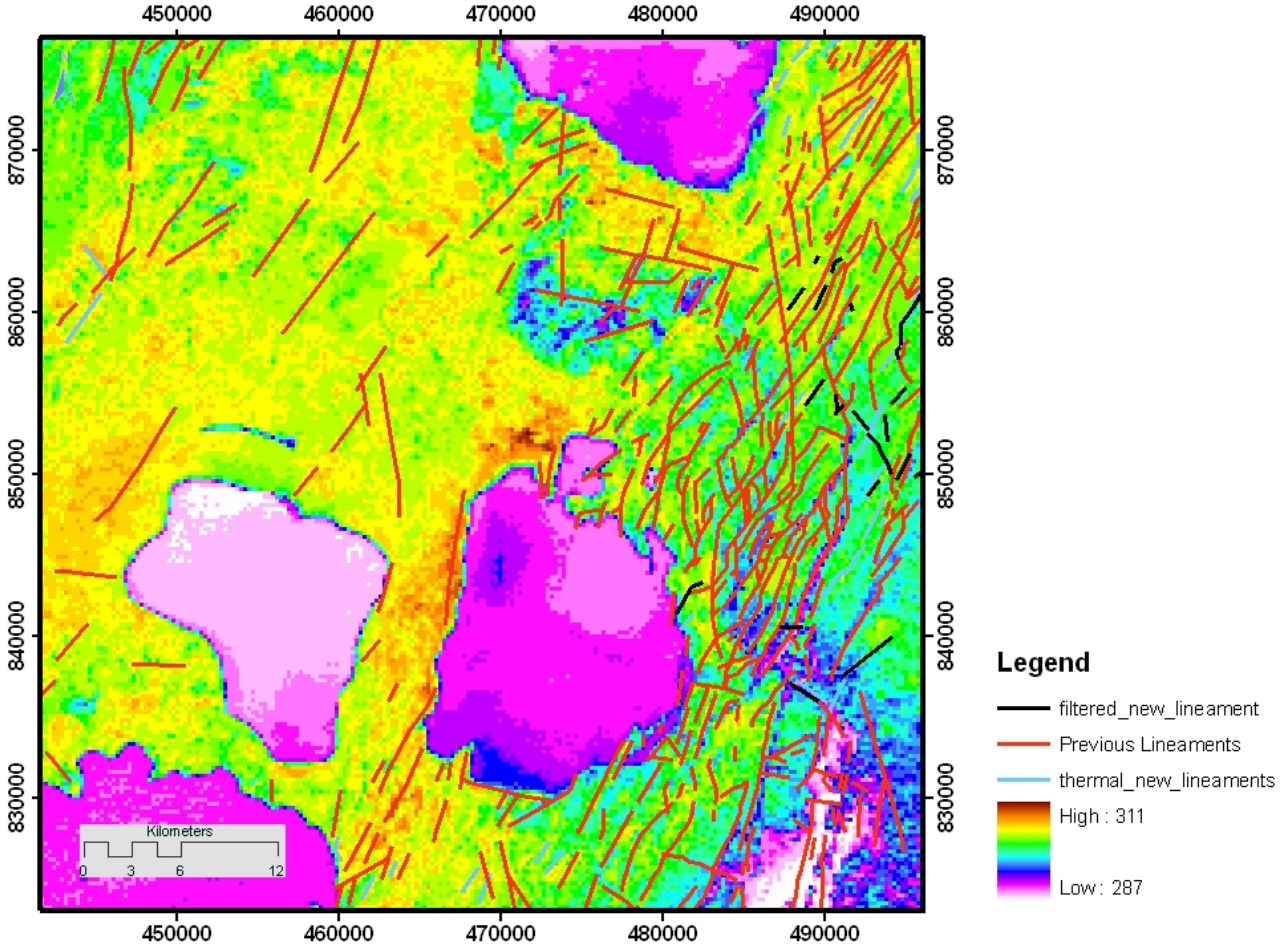

Figure 26: Relationship of lineaments with thermal map

From the relationship between lineaments and thermal mapping there can be seen that lineaments are align on the thermally anomalous areas. So that it is possible to extract the lineaments from the thermal maps. In this study lineaments extracted from the thermal maps. Figure 27 shows that red colored lineaments are extracted from the thermal map with the scale of 1:100000.

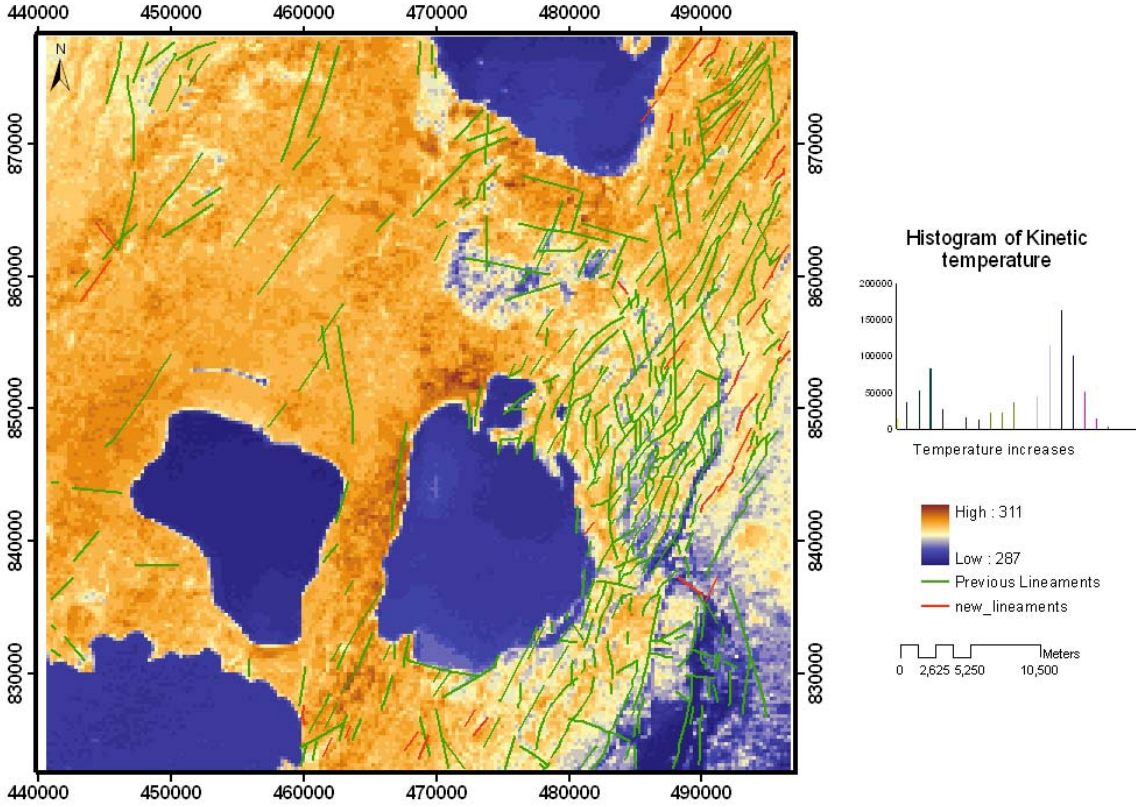

Figure 27: Additional lineaments extracted from the thermal map with the scale of 1:100000.

3.3. Thermal map with field observation

During field observation the thermal manifestation like hot springs are totally exposed on the top of Lake Langano which is south western side of Aluto Mountain (Figure 28). The thermally altered rocks and hot springs Figure 29 tells us that the place is a hot ground water discharged area from the highly thermally affected of the Aluto Mountain: this is facilitated by the lineaments that are found in the eastern part of Lake Langano and Aluto Mountain.

Figure 28: Thermally altered areas and hot springs observed during field work

Figure 29: Thermally altered rocks which affected by the hot spring which discharged from Aluto Mountain and eastern High lands.

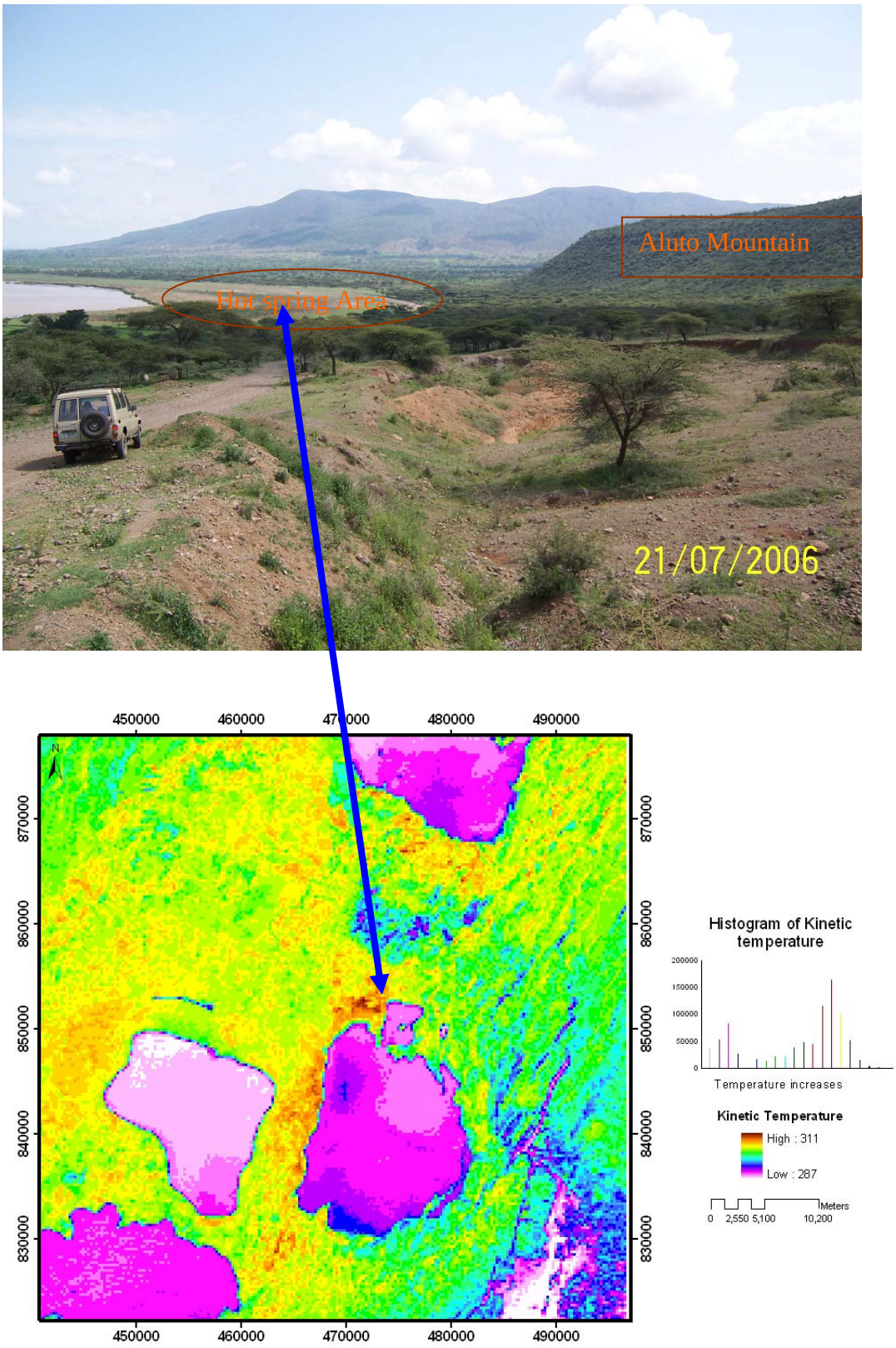

Figure 30: comparison of the thermal map obtained using satellite images with the field observed thermally high area

CHAPTER FOUR

Conclusions and Recommendations

Remote sensing and Geographic information system were applied to map thermal manifestations and lineament analysis based on the Visual Basic for application of ArcGIS software. Interpretation of LANDSAT 7 ETM+ thermal images were done to produce thermal maps. Lineament analysis produced lineament density and orientation maps. These outputs were overlaid together and compared with groundwater occurrences in the area.

Two approaches have been developed to recover Land Surface Temperature from multispectral TIR imagery (Schmugge et al., 1998). I have used the approach that utilizes a radiative transfer equation to correct the at-sensor radiance to surface radiance, followed by an emissivity model to separate the surface radiance into temperature and emissivity (Schmugge et al., 1998). Using this there is an anomaly of temperature in the study area and this tells us that there are hotspots which exhibit high temperature in the rift system. The high temperature areas, specifically in Aluto Volcanic center and Northern shore of Lake Langano, are most prominent areas of hydrothermal activities.

Lineament maps such as lineament density map are important to reveal the groundwater recharge, flow and development. Especially, groundwater flows and yields in mountainous areas comprised of fractures, joints and faults. Furthermore, the orientation of lineaments is also one of the important parameter to tell about the inter relation of the lineaments that is the intersection or the cross over of the lineaments. These areas may be the best areas to develop the productive well for the ground water occurrence. That is to say, these lineaments may give important information on the distribution of well development and management. Therefore, the lineament and related maps are considered as essential maps in basic groundwater surveys in the Ethiopian rift system.

VBA script has been used for the analysis of lineaments. With these data, the lineament density maps have been drawn. These density maps were integrated to the ground water table contour, to identify the direction of flow of ground water. From these it has been concluded that the lineaments act as a conduit for the groundwater flow since the density of the lineament decreases towards the rift floor from the escarpment in the study area (Figure 21, 22 and 23)

Directional filtering was applied on digital images to increase the visibility of linear features in specific directions. Moreover, in the study area thermal maps were also one of the methods used for the lineament extraction by interpreting the anomalous areas from the thermal map (Figure 26).

Recommendation has been set based on the observations and findings. The thermal mapping is one of the methods for extracting the lineaments in which identified in this study so that if there is a detail analysis would be made for the rest of the rift valley of Ethiopia, there will be a good clue for the analysis of the lineaments as well as for ground water assessment.

Having regional data of ground water table makes regional decision of ground water occurrence in the study. Therefore I recommend that if there is a detail data regarding the wells of the rift system, integration of the lineament analysis and thermal mapping would constitute the best tool for the determination of the ground water occurrence in the rift System (MER).

References

Arlegui, A.L., Soriano, M.A.,1998. Characterizing lineaments from satellite images and field and field studfies in the centeral Ebro basin (NE Spain). *International Journal of Remote Sensing* 19 (16), 3169-3185

Baker, B.H., Mohr, P.A., Williams, L.A.J., 1972. Geology of the eastern Rift System of Africa. Geol.Soc.Am.spec.Paper 136. 67 pp.

Bekele et al., 2000. Fracture pattern of the main Ethiopian rift area from land sat imagery and field observation with a scale of 1:500000.

Bobba, A.G., Bukata, R.P. and Jerome, J.H. ,1992. Digitally processed satellite data as a tool I detecting potential groundwater flow systems. *Journal of Hydrology* 131: 25-62

Caselles, V., Coll, C., Valor, E., 1995. Mapping land surface emmisivity using AVHRR data: Application to La Mancha, Spain. *Remote Sensing Reviews,* 12, 311-3330.

Cortès, A.L., Maestro, A., Soriano, M.A., Casas, A.M., 1998. Lineaments and fracturing in the Neogene rocks of the the Almazan Basin, northern Spain. Geological Magazine 135 (2), 255-268.

Dash, P.., Gottsche,F.-M.,Olesen, F.-S., & Fischer,H.,2002. Land Surface temperature and emmisivity estimation from passive sensor data: Theory and practice-current trends. *International Journal of Remote Sensing*, 23(13),2563-2594.

Fernandes, A.J., Rudolph, D.L., 2001. The influence of Cenozoic tectonics on the groundwater production capacity of fractured zones: A case study in Sao Paulo, Brazil. Hydrogeology Journal 9, 151-167.

Franca, G.B., & Cracknell, A.P.,1994.Retrieval of land and sea surface temperature using NOAA-H AVHRR data in north-eastern Brazil.International Journal of RemoteSensing,15, 1695 -1712

Friedl, M.A., 2002. Forward and inverse modeling of land surface energy balance using surface temperature measurements. *Remotesensing of Environment*,79,344-354.

Gasse, F. ,1980. Late Quaternary changes in the lake levels and diatom assemblages on the southeastern margin of the Sahara. Paleoecology of Africa 11:117–134.

Gasse, F. and Street, F.A. 1978. 'Late quaternary lake level fluctuations and environments of the northern Rift Valley and Afar Region (Ethiopia and Djibouti)', Palaeogeogr., Palaeoclim., Palaeoecol.24: 279-325.

Gianneli, G. and Meseret Teklemariam., 1993. Water-rock interaction processes in the Aluto-Langano geothermal field (Ethiopia).Jour.Volcano.Geotherm.Rese. 56: 429-445

Hardcastle, K.C., 1995. Photolineament factor: A new computer-aided method for remotely fractured. Photogrammetric Engineering &Remote Sensing 61 (6), 739-747.

Hobbs, W.H., 1904. Lineaments of the Atlantic border region Geological Society America Bulletin, 15: 483-506.

Irish, R.R., 2000, LANDSAT 7 science data user's handbook: http://ltpwww.gsfc.nasa.gov/IAS/handbook/handbook_toc.html, National Aeronautics and Space Administration.

Lattman, L.H., Parizek, R.R., 1964. Relationship between fracture traces and the occurrence of groundwater in carbonate roaks.Journal of Hydrology 2, 73 -91.

Lillesand and Ralph W. Kiefer, 1994: Remote sensing and image interpretation. John wiley and sons, New York,NY, thierd edition.

LLOYD, E.F. ,1977. : geological factors influencing geothermal exploration in Langano region, Ethiopia. Unpublished report for UN geothermal project in Ethiopia.

Mabee, S.B., Hardcastle, K.C., Wise, D.U., 1994. A method of collecting and analyzing lineaments for regional-scale fractured-bedrock aquifer studies. Ground Water 32 (6),884-894.

Magowe, M., Carr, J.R., 1999. Relationship between lineaments and ground water occurrence in western Botswana. Ground Water 37 (2), 282-286.

Makin et al., 1975. 'Development prospects in the southern Rift Valley of Ethiopia', Tolworth, Land resources DIV.U.K.Min. Overseas Devel.:270

Markham, B.L., and Barker, J.L., 1986, LANDSAT MSS and TM post-calibration dynamic ranges, exoatmospheric reflectances and at-satellite temperatures: EOSAT LANDSAT Technical Notes, v. 1, p. 3-8.

Meijerink, A.M.J., 1996. Remote sensing applications to hydrology : *Groundwater J.Hydrol.Sci.* 41(4): 549-561

Menenti,M., 1984. Physical aspects and determination of evaporation in deserts, applying remote sensing techniques. PhD Thesis, Wageningen Agr. Univ., ICW Publ. Wageningen.The Netherlands, 184 pp.

Mohammed, M.U. and Bonnefille, R.1991.'The recent history of vegetation and climate around Lake Langano',Paleocology of Africa 22:275-286

Nicolson, S.E. and Chervin, R.M. 1983.'Recent rainfall flactuations in Africa-Interhemispheric teleconnection ',Varations in the globbal water budget.As-Pe al.,W.Reidel:221-238

O'Leary, D.W. Friedman, J.D. nd Pohn, H.A. , 1976.Lineament, Linear Lineation some proposed new standards for old terms . Geological Society America Bulletin, 87.1463-1469.

Prata, A.J., 1993. Land surface temperatures derived from the advanced very high resolution radiometer and the along-track scanning radiometer: 1.Theory. *Jornal of Geophysical research*, 98, 16689-16702.

Prata, A. J., Caselles, V., Coll, C., Sobrino, J. A., & Ottle, C. (1995). Thermal remote sensing of land surface temperature from satellites: Current status and future prospects. *Remote Sensing Reviews*, 12, 175–224.

Quattrochi, D. A., & Goel, N. S., 1995 . Spatial and temporal scaling of thermal remote sensing data. *Remote Sensing Reviews*, 12, 255– 286.

Rothery, D.A., Francis, P.W.and Wood, C.A., 1988. Volcano monitoring using short wavelength infrared data from satellite. J. Geophys. Res.93:7993-8008.

Schmugge, T., Hook, S. J., & Coll, C., 1998. Recovering surface temperature and emissivity from thermal infrared multispectral data. *Remote Sensing of Environment*, 65, 121– 131.

Shimelis Fikre, 2006 . Hydrogeological system analysis in ziway-Shala lakes area using Hydrochemistry and Isotop techniques ,centeral Ethiopia. MSc thesis, Addis Ababa University, Ethiopia, 70.

Smith, R. M., 1986 . Comparing traditional methods for selecting class intervals on choroplth maps. Proffesional Geographer, 38 (1), 62-67

Snyder, W.C., Wan, Z., Zhang, Y., & Feng, Y. –Z., 1998 . Classification based emmisivity for land surface temperature measurement from space *International journal of remote sensing*,21,353-2774.

Tenalem Ayenew, 1998. The hydrogeological system of the lake district basin , centeral Main Ethiopian rift. PhD thesis, Free University of Amsterdam, The Netherlands, 259 pp.

United States Geological Survey (USGS)/EROS Data Center (EDC), L1-409, Level 1 Product Output Files Data Format Control Book, Volume 5, Book 2, Revision 4, January 2000

Valor, E., & Caselles, V., 1996. Mapping land surface emmisivity from NDVI: Application to European, African, and South American areas *Remote Sensing of Environment*, 57,167-184

Woldu, Z. and Taddesse, M.1990.'The vegetation in lakes regions of the rift valley of Ethiopia and the possiblity of its recoveries', SINET:Ethiopia Jornal of Science 13:97-120.

Appendix

Appendix 1: Visual basic Script for the lineament orientation analysis and mapping

```
'*****************************************************************************************************************
**

'It is used for calculating the orientation of lineaments and number of points (as
vertices ) that are ' present in each lineaments.
Sub CalculateKForPolyline()
Dim pMxDoc As IMxDocument
Set pMxDoc = ThisDocument
Dim pFlayerline As IFeatureLayer
Set pFlayerline = pMxDoc.FocusMap.Layer(1)
Dim pFClassline As IFeatureClass
Set pFClassline = pFlayerline.FeatureClass
Dim pPtColl As IPointCollection
Dim pFCursor As IFeatureCursor
Set pFCursor = pFClassline.Search(Nothing, False)
Dim pFeatureLine As IFeature
Set pFeatureLine = pFCursor.NextFeature
Dim pFields As IFields
Dim pfield As IField
Set pFields = pFClassline.Fields
Dim IndexOrientation As Long
IndexOrientation = pFields.FindField("Orient")
Dim IndexNumPnts As Long
IndexNumPnts = pFields.FindField("NumPnts")
'Set pField = pFields.Field(IndexNumPnts)
Dim NumOfPoints As Integer
Dim X() As Double
```

```
Dim Y() As Double
Dim SigmaX As Double, SigmaY As Double, SigmaXY As Double, SigmaX2 As
Double
Dim SlopeK As Double
Dim Orientation As Double
Dim i As Integer
'Start editor
While Not pFeatureLine Is Nothing
  Set pPtColl = pFeatureLine.ShapeCopy
  NumOfPoints = pPtColl.PointCount
  SlopeK = 0
  ReDim X(NumOfPoints - 1)
  ReDim Y(NumOfPoints - 1)
  'Close #1
  'Open "c:\temp\test.txt" For Output As #1
  For i = 0 To NumOfPoints - 1
   X(i) = pPtColl.Point(i).X
   Y(i) = pPtColl.Point(i).Y
   'Print #1, X(i), Y(i)
  Next i
  'Close #1
  If NumOfPoints = 2 Then
   If X(1) = X(0) Then
    Orientation = 3.14159265 / 2
   Else
    SlopeK = (Y(1) - Y(0)) / (X(1) - X(0))
    Orientation = Atn(SlopeK)
   End If
  Else
   SigmaX = 0
   SigmaY = 0
```

```
    SigmaXY = 0
    SigmaX2 = 0
    For i = 0 To NumOfPoints - 1
     SigmaX = SigmaX + X(i)
     SigmaY = SigmaY + Y(i)
     SigmaXY = SigmaXY + X(i) * Y(i)
     SigmaX2 = SigmaX2 + X(i) ^ 2
    Next i
    SlopeK = (NumOfPoints * SigmaXY - SigmaX * SigmaY) / (NumOfPoints *
SigmaX2 - SigmaX ^ 2)
    Orientation = VBA.Atn(SlopeK)
   End If
   Orientation = Orientation / 3.1415926 * 180
   pFeatureLine.Value(IndexOrientation) = Orientation
   pFeatureLine.Value(IndexNumPnts) = NumOfPoints
   pFeatureLine.Store
   Set pFeatureLine = pFCursor.NextFeature
Wend
End Sub

'*****************************************************************************************
**********************
```

Appendix 2: Visual basic Script for the lineament length density analysis and mapping

```
'BINYAM December 16, 2006 reprogrammed to calculate dens_len (which is
the density of lineament length per area of each polygon)

Sub CalculateFractureDensity_LEN2()
```

```
Dim pMxDoc As IMxDocument
Set pMxDoc = ThisDocument
Dim pMap As IMap ' Binyam Dec 05,2006
Set pMap = pMxDoc.FocusMap ' Binyam dec 05, 2006
Dim pFlayerPolygon As IFeatureLayer
Set pFlayerPolygon = pMxDoc.FocusMap.Layer(0)
Dim pFClassPolygon As IFeatureClass
Set pFClassPolygon = pFlayerPolygon.FeatureClass
Dim pFlayerPolyLine As IFeatureLayer
Set pFlayerPolyLine = pMxDoc.FocusMap.Layer(1)
Dim pFClassPolyLine As IFeatureClass
Set pFClassPolyLine = pFlayerPolyLine.FeatureClass
Dim pPolyLineFields As IFields
Set pPolyLineFields = pFClassPolyLine.Fields
Dim IndexOrder As Long
IndexOrder = pPolyLineFields.FindField("Order_No")
Dim pLENGTH As Long
pLENGTH = pPolyLineFields.FindField("SHAPE_LENGTH")
Dim pFCursorGon As IFeatureCursor
Set pFCursorGon = pFClassPolygon.Search(Nothing, False) ' Binyam dec
05,2006
Dim pFeatGon As IFeature
Set pFeatGon = pFCursorGon.NextFeature
Dim pFCursorLine As IFeatureCursor
Dim pSpatialFilter As ISpatialFilter
Set pSpatialFilter = New SpatialFilter
Dim pFeatLine As IFeature
Dim pCount As Double
Dim pFields As IFields
Dim pfield As IField ' binyam dec 05,2005
Dim parea As IArea
```

```
'Dim pFieldNum As IField
'Dim pFieldLen As IField
 Set pFields = pFClassPolygon.Fields
 Dim IndexDensNum As Long
 IndexDensNum = pFields.FindField("Dens_Num")
 Dim IndexDensLen As Double
 IndexDensLen = pFields.FindField("Dens_Len")

 Dim WNum As Integer
 While Not pFeatGon Is Nothing
  Set parea = pFeatGon.Shape
  With pSpatialFilter
  Set .Geometry = pFeatGon.ShapeCopy
      .GeometryField = "Shape"
      .SpatialRel = esriSpatialRelIntersects
  End With
  Set pFCursorLine = pFClassPolyLine.Search(pSpatialFilter, False)
  Set pFeatLine = pFCursorLine.NextFeature
  pCount = 0
```

‘pCount is computed from the given coded values based on the length of the lineaments that are present in the study area.

‘1.2: For the lineaments that have length Greater than 10000 meters.

‘1.5: For the lineaments that have length between 5000 meters and 10000 meters.

‘2.0:For the lineaments that have length less than 5000 meters.

```
  While Not pFeatLine Is Nothing
   If pFeatLine.Value(pLENGTH) > 10000 Then
    pCount = pCount + 1.2 * pFeatLine.Value(pLENGTH)
```

```
  ElseIf pFeatLine.Value(pLENGTH) > 5000 And pFeatLine.Value(pLENGTH)
< 10000 Then
    pCount = pCount + 1.5 * pFeatLine.Value(pLENGTH)
  ElseIf pFeatLine.Value(pLENGTH) > 0 And pFeatLine.Value(pLENGTH) <
1000 Then
    pCount = pCount + 2 * pFeatLine.Value(pLENGTH)
  Else
    pCount = pCount + 1 * pFeatLine.Value(pLENGTH)
  End If
  Set pFeatLine = pFCursorLine.NextFeature
 Wend
 Dim denslen As Double
 denslen = pCount / parea.Area * 10 ^ 6
pFeatGon.Value(IndexDensLen) = denslen ' Binyam dec 05 ,2006
 pFeatGon.Store
Debug.Print pCount
Debug.Print denslen
Set pFeatGon = pFCursorGon.NextFeature
Wend
End Sub

'*****************************************************************************************
**********************
```

Appendix 3: Visual basic Script for the lineament number density analysis and mapping

'The following code calculates the fracture number density per a specified girded polygon.

```
Sub CalculateFractureDensity_num()
 Dim pMxDoc As IMxDocument
 Set pMxDoc = ThisDocument
 Dim pMap As IMap ' Binyam Dec 05,2006
 Set pMap = pMxDoc.FocusMap ' Binyam dec 05, 2006
 Dim pFlayerPolygon As IFeatureLayer
 Set pFlayerPolygon = pMxDoc.FocusMap.Layer(0)
 Dim pFClassPolygon As IFeatureClass
 Set pFClassPolygon = pFlayerPolygon.FeatureClass
 Dim pFlayerPolyLine As IFeatureLayer
 Set pFlayerPolyLine = pMxDoc.FocusMap.Layer(1)
 Dim pFClassPolyLine As IFeatureClass
 Set pFClassPolyLine = pFlayerPolyLine.FeatureClass
 Dim pPolyLineFields As IFields
 Set pPolyLineFields = pFClassPolyLine.Fields
 Dim IndexOrder As Long
 IndexOrder = pPolyLineFields.FindField("Order_No")
 Dim pFCursorGon As IFeatureCursor
 Set pFCursorGon = pFClassPolygon.Search(Nothing, False) ' Binyam dec
05,2006
 Dim pFeatGon As IFeature
 Set pFeatGon = pFCursorGon.NextFeature
 Dim pFCursorLine As IFeatureCursor
 Dim pSpatialFilter As ISpatialFilter
 Set pSpatialFilter = New SpatialFilter
 Dim pFeatLine As IFeature
 Dim pCount As Long
 Dim pFields As IFields
 Dim pfield As IField ' binyam dec 05, 2005
 Dim parea As IArea
'Dim pFieldNum As IField
```

```
'Dim pFieldLen As IField
 Set pFields = pFClassPolygon.Fields
 Dim IndexDensNum As Long
 IndexDensNum = pFields.FindField("Dens_Num")
 Dim IndexDensLen As Long
 IndexDensLen = pFields.FindField("Dens_Len")

 Dim WNum As Integer
 While Not pFeatGon Is Nothing
  Set parea = pFeatGon.Shape
  With pSpatialFilter
  Set .Geometry = pFeatGon.ShapeCopy
      .GeometryField = "Shape"
      .SpatialRel = esriSpatialRelIntersects
  End With
  Set pFCursorLine = pFClassPolyLine.Search(pSpatialFilter, False)
  Set pFeatLine = pFCursorLine.NextFeature
  pCount = 0
```

‘ pCount is computed from the given coded values that are given on the lineaments attribute ‘table as IndexOrder field name.

‘ IndexOrder = 1 for the lineaments that have length Greater than 10000 meters.

‘IndexOrder = 2 for the lineaments that have length between 5000 meters and 10000 meters.

‘ IndexOrder = 3 for the lineaments that have length less than 5000 meters.

```
  While Not pFeatLine Is Nothing
   If pFeatLine.Value(IndexOrder) = 1 Then
    pCount = pCount + 1.2
   ElseIf pFeatLine.Value(IndexOrder) = 2 Then
```

```
  pCount = pCount + 1.5
 ElseIf pFeatLine.Value(IndexOrder) = 3 Then
  pCount = pCount + 2#
 Else
  pCount = pCount + 1
 End If
 Set pFeatLine = pFCursorLine.NextFeature
Wend
Dim dens As Double
dens = pCount / parea.Area * 10 ^ 6
pFeatGon.Value(IndexDensNum) = dens ' Binyam dec 05 ,2006
pFeatGon.Store
Debug.Print pCount
Debug.Print dens
 'MsgBox "Lineaments with in the Polygon:" & vbCrLf & pCount 'binyam dec
03,2006
 Set pFeatGon = pFCursorGon.NextFeature
Wend
End Sub
```

Appendix 4: ground water sample data and their location from different well data in the study area (Source: Shimelis 2006)

MAJOR_CODE	TYPE	CODE_	TYPE	LABEL	X	Y
Sub_Group-1	Bore_Hole	SB1-20	BH-50	9	489000	860000
Sub_Group-1	Cold_Spring	SB1-3	CS-22	75	476797	850890
Sub_Group-1	Cold_Spring	SB1-4	CS-23	76	470839	851126
Sub_Group-1	HotSpring	SB1-13	HS-27	22	476071	852375
Sub_Group-1	HotSpring	SB1-14	HS28	23	469455	850822
Sub_Group-2	Bore_Hole	SB2-15	BH-30	37	459810	832677
Sub_Group-2	Bore_Hole	SB2-24	BH-43	45	486788	867554
Sub_Group-2	Bore_Hole	SB2-27	BH-46	47	462304	867052
Sub_Group-2	Bore_Hole	SB2-31	BH-50	51	478715	828088
Sub_Group-2	Bore_Hole	SB2-39	BH-65	58	489060	838182
Sub_Group-2	Bore_Hole	SB2-43	BH-81	61	467183	868410
Sub_Group-2	Cold_Spring	SB2-51	CS-19	72	476206	852307
Sub_Group-2	Cold_Spring	SB2-53	CS-21	74	478784	846641
Sub_Group-2	Cold_Spring	SB2-54	CS-27	77	479186	846962
Sub_Group-2	Geothermal_well	SB2-56	GTW-1	114	473069	857081
Sub_Group-2	Geothermal_well	SB2-57	GTW-2	101	473130	861620
Sub_Group-2	Hand_Dug_Well	SB2-63	DW-13	88	460633	853379
Sub_Group-2	Hand_Dug_Well	SB2-67	DW-2	92	463082	855772
Sub_Group-2	HotSpring	SB2-58	HS-26	102	478784	846641
Sub_Group-3	Bore_Hole	SB3-3	BH-17	107	467974	863049
Sub_Group-3	Bore_Hole	SB3-5	BH-19	108	470160	868877
Sub_Group-3	Bore_Hole	SB3-6	BH-20	109	466726	839869
Sub_Group-3	Bore_Hole	SB3-7	BH-21	110	467649	866929
Sub_Group-3	Geothermal_well	SB3-11	GTW-1	114	473069	857081
Sub_Group-3	Hand_Dug_Well	SB3-8	DW-36	111	469472	871897
Sub_Group-4	Bore_Hole	SB4-1	BH-29	115	464400	838560
Sub_Group-4	HotSpring	SB4-2	HS-2	116	460229	825336

Sub_Group-4	HotSpring	SB4-3	HS-9	117	459882	825336
Sub_Group-5	Geothermal_well	SB5-2	GTW-4	119	484614	857721
Sub_Group-5	Geothermal_well	SB5-3	GTW-5	120	484888	854858
Sub_Group-5	Geothermal_well	SB5-4	GTW-7	121	482908	854827
Sub_Group-5	Geothermal_well	SB5-5	GTW-8	122	481995	863631
Sub_Group-5	HotSpring	SB5-6	HS-10	123	474644	852428
Sub_Group-5	HotSpring	SB5-7	HS-4	124	475903	848260
Sub_Group-6	Geothermal_well	SB6-1	GTW-3	126	481477	857142
Sub_Group-6	Geothermal_well	SB6-2	GTW-6	127	482543	859762
Sub_Group-6	HotSpring	SB6-3	HS-3	128	476380	852515
Sub_Group-7	Hand_Dug_Well	SB7-1	DW-17	129	464706	855772
Sub_Group-7	therma_Grad_well	SB7-3	TW-2	131	480927	855133
Sub_Group-7	therma_Grad_well	SB7-4	TW-4	132	481672	854871

Appendix 5: Scripts that are used for the thermal mapping in ERDAS IMAGINE 8.6 software

1. Calculation of getting At satellite temperature

" *$n1_studyb6h* is the image of LANDSAT 7 thermal band high gain mode
" *$n3_radianceb6h* is the image computed from the thermal band high gain mode
" *n4_radiancetempb6h* is the at satellite temperature

```
COMMENT "Generated from graphical model: d:/images/radiant_temperature_band6h .gmd";

#
# Declarations
#
Integer RASTER n1_studyb6h FILE OLD NEAREST NEIGHBOR AOI NONE "d:/images2/studyb6h.img";
Float RASTER n3_radianceb6h FILE NEW USEALL ATHEMATIC FLOAT DOUBLE "d:/images2/radianceb6h.img";
Integer RASTER n4_radiancetempb6h FILE NEW USEALL ATHEMATIC 16 BIT UNSIGNED INTEGER "d:/images2/radiancetempb6h.img";
#
# Function definitions
#
n3_radianceb6h = (((12.65 - 3.2) / (255 - 1)) * ($n1_studyb6h - 1) + 0) - 0.31;
n4_radiancetempb6h = 1282.71 / LOG ( (666.09 / $n3_radianceb6h) + 1 );
QUIT;
```

2. Calculation of getting emmisivity corrected at satellite temperature

« *n3_emmis_corr_tempb6h* is the emmisivity corrected image
« *$n1_radiancetempb6h* is at satellite temperaure used for calculating emmisivity corrected image

```
COMMENT "Generated from graphical model: d:/images/emmisivitycorrmodelb6l.gmd";

# Declarations
#
Integer RASTER n1_radiancetempb6h FILE OLD NEAREST NEIGHBOR AOI NONE "d:/images2/radiancetempb6h.img";
Integer RASTER n3_veg_emmis_corr_tempb6h FILE NEW USEALL
```

ATHEMATIC 16 BIT UNSIGNED INTEGER "d:/images2/veg_emmis_corr_tempb6h.img";

#
Function definitions
#
n3_emmis_corr_tempb6h = *$n1_radiancetempb6h* / (1 + (0.00115 * *$n1_radiancetempb6h*/ 1.438) * 0.041);

QUIT;

3. Calculation script for kinetic surface temperature

"*$n6_ndvi* is the image of Normalized difference Vegetative Index
"*n1_1emmisivity* is emmisivity image that is computed from NDVI
"$n4_2temperatureb6l is the emmisivity corrected at satellite temperature for calculating kinetic temperature
"n3_1tempkin is the image shows the surface kinetic temperature.

COMMENT "Generated from graphical model: d:/images/kintempmodel.gmd";
#
Declarations
#
Integer RASTER n1_1emmisivity FILE NEW USEALL ATHEMATIC 16 BIT UNSIGNED INTEGER "d:/images/1emmisivity.img";
Integer RASTER n3_1tempkin FILE NEW USEALL ATHEMATIC 16 BIT UNSIGNED INTEGER "d:/images/1tempkin.img";
Integer RASTER n4_2temperatureb6l FILE OLD CUBIC CONVOLUTION AOI NONE "d:/images/2temperatureb6l.img";
Float RASTER n6_ndvi FILE OLD NEAREST NEIGHBOR AOI NONE "d:/images/ndvi.img";
#
Function definitions
#
n1_1emmisivity = CONDITIONAL { *($n6_ndvi* < 0.16) 0 , (0.16 < *$n6_ndvi* < 0.74) 1.009 + 0.047 * LOG (*$n6_ndvi*) *,($n6_ndvi* > 0.74)0 } ;
n3_1tempkin = *$n4_2temperatureb6l* / SQRT (SQRT (*$n1_1emmisivity*)) ;
QUIT;

Appendix 6: Ground water table data for the determination ground water flow and relation with lineaments

BH-1	Easting	Northing	Ground Water level (meters)
BH-2	511000	856242	151
BH-3	510944	862096	125
BH-4	515055	866097	168
BH-5	514701	870557	115
BH-6	520076	882997	105
BH-7	519294	884778	120
BH-8	455519	798303	145
BH-9	412288	830368	145
BH-10	431494	841849	186
BH-11	429285	849711	-
BH-12	440615	852123	85
BH-13	464529	814467	109
BH-14	459185	902574	122
BH-15	501805	895996	102
BH-16	462853	870941	71
BH-17	461786	852249	71